Senolytic CAR T cells reverse senescence-associated pathologies

https://doi.org/10.1038/s41586-020-2403-9

Received: 24 September 2019

Accepted: 6 May 2020

Published online: 17 June 2020

Check for updates

Corina Amor[1,2,12], Judith Feucht[3,4,12], Josef Leibold[2,12], Yu-Jui Ho[2], Changyu Zhu[2], Direna Alonso-Curbelo[2], Jorge Mansilla-Soto[3,4], Jacob A. Boyer[1,5], Xiang Li[2,6], Theodoros Giavridis[3,4], Amanda Kulick[5], Shauna Houlihan[2], Ellinor Peerschke[7], Scott L. Friedman[8], Vladimir Ponomarev[9], Alessandra Piersigilli[10], Michel Sadelain[3,4]✉ & Scott W. Lowe[2,11]✉

Cellular senescence is characterized by stable cell-cycle arrest and a secretory program that modulates the tissue microenvironment[1,2]. Physiologically, senescence serves as a tumour-suppressive mechanism that prevents the expansion of premalignant cells[3,4] and has a beneficial role in wound-healing responses[5,6]. Pathologically, the aberrant accumulation of senescent cells generates an inflammatory milieu that leads to chronic tissue damage and contributes to diseases such as liver and lung fibrosis, atherosclerosis, diabetes and osteoarthritis[1,7]. Accordingly, eliminating senescent cells from damaged tissues in mice ameliorates the symptoms of these pathologies and even promotes longevity[1,2,8–10]. Here we test the therapeutic concept that chimeric antigen receptor (CAR) T cells that target senescent cells can be effective senolytic agents. We identify the urokinase-type plasminogen activator receptor (uPAR)[11] as a cell-surface protein that is broadly induced during senescence and show that uPAR-specific CAR T cells efficiently ablate senescent cells in vitro and in vivo. CAR T cells that target uPAR extend the survival of mice with lung adenocarcinoma that are treated with a senescence-inducing combination of drugs, and restore tissue homeostasis in mice in which liver fibrosis is induced chemically or by diet. These results establish the therapeutic potential of senolytic CAR T cells for senescence-associated diseases.

Given the contribution of senescence to tissue damage, there is growing interest in the development of 'senolytic' agents that selectively eliminate senescent cells[12]. Several small molecules exhibit senolytic activity, but most lack potency and produce substantial side effects[1,12,13]. An alternative approach could involve CAR T cells directed against senescence-specific surface antigens. CARs are synthetic receptors that redirect T cell specificity, effector potential and other functions[14]. CAR T cells that target CD19 have shown notable efficacy in patients with refractory B cell malignancies[15], and other cell-surface antigens show promise as targets for CAR therapy in different contexts[16–18]. Here we investigate whether CAR T cells could serve as senolytic agents.

Upregulation of uPAR during senescence

To identify cell-surface proteins that are broadly and specifically upregulated in senescent cells, we compared RNA-sequencing (RNA-seq) datasets derived from three independent and robust models of senescence: 1) therapy-induced senescence in mouse lung adenocarcinoma *Kras*^{G12D};*p53*$^{-/-}$ (KP) cells (*p53* is also known as *Trp53*) that are triggered to senesce by a combination of MEK inhibition and CDK4 and CDK6 (CDK4/6) inhibition[19]; 2) oncogene-induced senescence in mouse hepatocytes, mediated by the in vivo delivery of *Nras*^{G12V} through hydrodynamic tail vein injection (HTVI)[4]; and 3) culture-induced senescence in mouse hepatic stellate cells (HSCs) (Extended Data Fig. 1a). We focused on transcripts that encode molecules that are located in the plasma membrane (as determined by UniProtKB) and that were upregulated in all datasets (Extended Data Fig. 1b, c). Eight transcripts were identified, which encode proteins related to extracellular matrix remodelling or the coagulation cascade (Extended Data Fig. 1d).

Given that ideal antigens for the engagement of CAR T cells should be highly expressed on target cells but not in vital tissues, we ranked each transcript according to its magnitude of upregulation ($\log_2$(expression in senescent cells/expression in non-senescent cells)), and then excluded those that were highly expressed in vital tissues (as determined by the Human Protein Atlas and the Human Proteome Map)[20]. This process identified *PLAUR*, which encodes the

[1]Louis V. Gerstner Jr Graduate School of Biomedical Sciences, Memorial Sloan Kettering Cancer Center, New York, NY, USA. [2]Department of Cancer Biology and Genetics, Sloan Kettering Institute, Memorial Sloan Kettering Cancer Center, New York, NY, USA. [3]Center for Cell Engineering, Memorial Sloan Kettering Cancer Center, New York, NY, USA. [4]Immunology Program, Sloan Kettering Institute, Memorial Sloan Kettering Cancer Center, New York, NY, USA. [5]Molecular Pharmacology and Chemistry Program, Memorial Sloan Kettering Cancer Center, New York, NY, USA. [6]Weill Cornell Graduate School of Medical Sciences, New York, NY, USA. [7]Department of Laboratory Medicine, Memorial Sloan Kettering Cancer Center, New York, NY, USA. [8]Division of Liver Diseases, Icahn School of Medicine at Mount Sinai, New York, NY, USA. [9]Department of Radiology, Memorial Sloan Kettering Cancer Center, New York, NY, USA. [10]Laboratory of Comparative Pathology, Rockefeller University, Weill Cornell Medicine and Memorial Sloan Kettering Cancer Center, New York, NY, USA. [11]Howard Hughes Medical Institute, Chevy Chase, MD, USA. [12]These authors contributed equally: Corina Amor, Judith Feucht, Josef Leibold. ✉e-mail: m-sadelain@ski.mskcc.org; lowes@mskcc.org

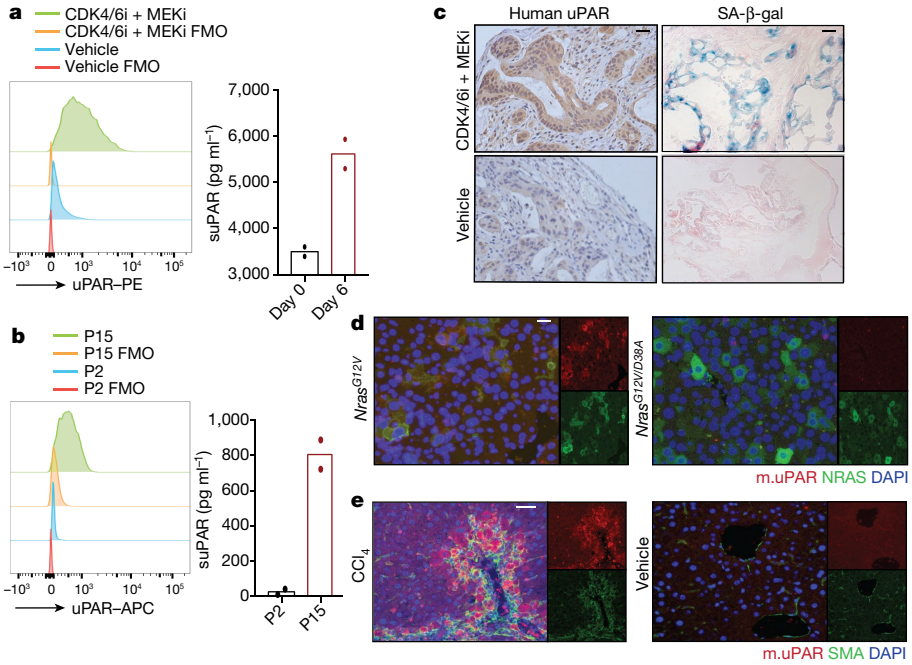

Fig. 1 | uPAR is a cell-surface and secreted biomarker of senescence. a, Left, flow cytometry analysis of uPAR expression on mouse KP lung adenocarcinoma cells after induction of senescence by treatment with MEK and CDK4/6 inhibitors (CDK4/6i + MEKi) as compared to controls. FMO, fluorescence minus one control. Representative results of $n = 3$ independent experiments. Right, levels of suPAR as determined by enzyme-linked immunosorbent assay (ELISA) in the supernatant of senescent or proliferating KP cells. Representative results of $n = 2$ independent experiments. **b**, Left, flow cytometry analysis comparing uPAR expression on primary human melanocytes after induction of senescence by continuous passage (P) with proliferating controls. Representative results of $n = 2$ independent experiments. Right, levels of suPAR in the supernatant of senescent (passage 15; P15) or proliferating (passage 2; P2) primary human melanocytes. Representative results of $n = 2$ independent experiments. **c**, Immunohistochemical staining of human uPAR and SA-β-gal in a patient-derived xenograft from human lung adenocarcinoma orthotopically injected into NSG mice and treated with vehicle or combined MEK and CDK4/6 inhibitors. Representative of $n = 2$ independent experiments ($n = 3$ mice per group). Scale bars, 50 µm. **d**, Co-immunofluorescence staining of uPAR (red) and NRAS (green) in the livers of mice six days after transfection by HTVI with a plasmid encoding $Nras^{G12V}$ or $Nras^{G12V/D38A}$. Representative results of $n = 3$ independent experiments ($n = 5$ mice per group). Scale bar, 50 µm. **e**, Co-immunofluorescence staining of uPAR (red) and smooth muscle actin (SMA; green) in the livers of mice six weeks after intraperitoneal treatment twice weekly with CCl_4 ($n = 7$ mice) or vehicle ($n = 4$ mice). Representative results of $n = 3$ independent experiments. Scale bar, 50 µm.

urokinase-type plasminogen activator receptor (uPAR), as a suitable candidate (Extended Data Fig. 1e). Accordingly, *PLAUR* was also upregulated in public datasets of senescent human cells[19,21] and immunohistochemistry confirmed that uPAR protein was absent in many vital organs (Extended Data Fig. 1g, f). Consistent with previous reports, low uPAR expression was detected in the bronchial epithelium. Other cell types that express uPAR include subsets of monocytes, macrophages and neutrophils[11,22].

uPAR is the receptor for urokinase-type plasminogen activator, which promotes the degradation of the extracellular matrix during fibrinolysis, wound healing or tumorigenesis[11]. uPAR also functions as a signalling receptor that promotes the motility, invasion and survival of tumour cells[11]. Nonetheless, mice that lack uPAR are viable and fertile[23]. A portion of uPAR is proteolytically cleaved upon ligand binding, which generates soluble uPAR (suPAR). Notably, suPAR is secreted by senescent cells as part of the senescence-associated secretory phenotype (SASP)[24] and serves as a serum biomarker for kidney disease and diabetes[25]—two chronic pathologies that are linked to senescence[25].

We next confirmed that uPAR expression was induced on the surface of senescent cells in vitro and in vivo. First, we evaluated therapy-induced senescence in mouse KP lung cancer cells that were treated with combined MEK and CDK4/6 inhibition, and replication-induced senescence in human primary melanocytes (Fig. 1a, b, Extended Data Fig. 2a, b). In both models, cell-surface expression of uPAR and supernatant suPAR levels were markedly increased after the induction of senescence (Fig. 1a, b). Second, we examined a patient-derived xenograft model of non-small-cell lung cancer in which mice were treated with combined MEK and CDK4/6 inhibitors[19] (Fig. 1c) and two different models of oncogene-induced senescence triggered either by the overexpression of $Nras^{G12V}$ in mouse hepatocytes transfected by HTVI (Fig. 1d, Extended Data Fig. 2c–e) or by the endogenous expression of $Kras^{G12D}$ in a mouse model of senescent pancreatic intraepithelial neoplasia (Extended Data Fig. 2f–i). Finally, we included a mouse model of carbon tetrachloride (CCl_4)-induced liver fibrosis, in which senescent HSCs contribute to the pathophysiology[6] (Fig. 1e, Extended Data Fig. 2j–m). In each system, the senescence-inducing treatment led to an increase in the number of uPAR-positive cells and an increase in serum suPAR levels. Notably, uPAR-positive cells did not express the proliferation marker Ki-67, but co-expressed interleukin 6 (IL-6)—an established component of the SASP[1,2].

We next confirmed that uPAR is highly expressed in tissues from patients with senescence-associated disorders. High levels of uPAR expression were observed in specimens of liver fibrosis of different aetiologies. uPAR-positive cells showed the same histological presentation as cells that expressed senescence-associated β-galactosidase (SA-β-gal), and co-expressed the senescence-associated markers p16 and IL-6 (Extended Data Fig. 3a, b). uPAR was also highly expressed in atherosclerotic plaques from human carotid endarterectomy specimens and in pancreatic intraepithelial neoplasia lesions from patients with pancreatic cancer (Extended Data Fig. 3c, d). In addition, increased levels of uPAR and/or suPAR have been noted in patients with other diseases that are associated with senescence, including osteoarthritis, diabetes and idiopathic pulmonary fibrosis[26–28]. Collectively, these results show that uPAR is a candidate target for senolytic CAR T cells.

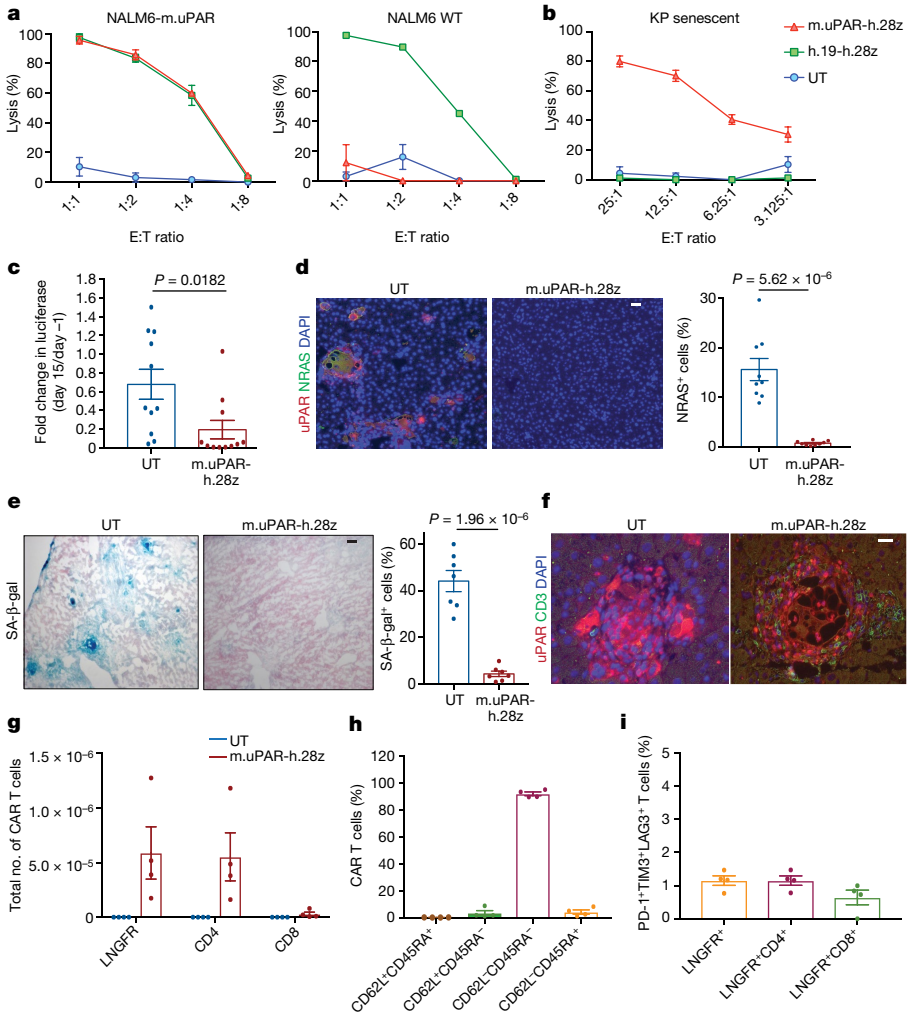

Fig. 2 | uPAR CAR T cells are bona fide senolytic agents. a, Cytotoxic T cell activity as determined by an 18-h bioluminescence assay using luciferase-expressing wild-type (WT) NALM6 cells or NALM6 cells that overexpress mouse uPAR (NALM6-m.uPAR) as targets. E:T ratio, effector-to-target ratio; UT, untransduced T cells. Data are representative of $n = 3$ independent experiments, each performed in triplicate. **b**, Cytotoxic T cell activity as determined by a 4-h bioluminescence assay using KP cells as targets in which senescence was induced by MEK and CDK4/6 inhibition. Data are representative of $n = 2$ independent experiments, each performed in triplicate. **c**–**i**, NSG mice were injected with a plasmid encoding $Nras^{G12V}$-GFP-luciferase and treated with 0.5×10^6 m.uPAR-h.28z CAR T cells or untransduced T cells 10 days after injection. Mice were euthanized 15 days later and livers were analysed. **c**, Fold change in luciferase signal in mice (calculated as the average radiance on day 15 divided by the average radiance on day −1) ($n = 11$ mice per group). **d**, Co-immunofluorescence staining of uPAR (red) and NRAS (green) and quantification of NRAS-positive cells ($n = 9$ mice per group). Scale bar, 50 µm. **e**, Representative staining and quantification of SA-β-gal-positive cells ($n = 7$ mice per group). Scale bar, 50 µm. **f**, Co-immunofluorescence staining of uPAR (red) and human CD3 (green), showing T cell infiltration ($n = 5$ mice per group). Scale bar, 50 µm. **g**–**i**, Number of liver-infiltrating CAR T cells (**g**), expression of CD62L and CD45RA (**h**) and percentage of PD-1$^+$TIM3$^+$LAG3$^+$ CAR T cells (**i**) among m.uPAR-h.28z CAR T cells as determined by flow cytometry ($n = 4$ mice per group). Representative results of $n = 2$ independent experiments (**c**–**f**). Data are mean ± s.e.m.; two-tailed unpaired Student's *t*-test (**c**–**e**).

Senolytic activity of uPAR CAR T cells

We constructed a uPAR-specific CAR comprising an anti-mouse uPAR (m.uPAR) single-chain variable fragment linked to human CD28 costimulatory and CD3ζ (h.28z) signalling domains (m.uPAR-h.28z), transduced human T cells and performed cytotoxicity assays using target cells that express a mouse uPAR cDNA (Extended Data Fig. 4a–d). To enable comparisons to well-characterized CAR T cells directed against CD19[29], mouse uPAR was introduced into the human CD19$^+$ pre-B acute lymphoblastic leukaemia (B-ALL) cell line NALM6 (Extended Data Fig. 4c). m.uPAR-h.28z CAR T cells showed no cytotoxicity towards uPAR-negative NALM6 cells, but comparable activity to CD19-specific CAR T cells incorporating human CD28 and CD3ζ signalling elements (h.19-h.28z) when targeting uPAR-expressing NALM6 cells (Fig. 2a, Extended Data Fig. 4d). m.uPAR-h.28z—but not h.19-h.28z—CAR T cells efficiently eliminated senescent KP cells that express endogenous uPAR, and this was accompanied by antigen-specific secretion of granzyme B and interferon γ (IFNγ) (Fig. 2b, Extended Data Fig. 4e). Hence, m.uPAR-h.28z CAR T cells can selectively and efficiently target senescent cells.

To study whether m.uPAR-h.28z CAR T cells could function as a bona fide senolytic agent in vivo, we took advantage of the well-characterized model of oncogene-induced senescence triggered by the hepatic overexpression of $Nras^{G12V}$-luciferase used above[4]. Although these senescent cells normally undergo SASP-mediated immune clearance[4], they are retained in the livers of immunodeficient NOD scid gamma (NSG) mice[4]. Successful transfection of *Nras*^{G12V} into hepatocytes of NSG mice was confirmed by bioluminescence imaging, and was followed by administration of 0.5×10^6 m.uPAR-h.28z CAR T cells or untransduced T cells as controls (Extended Data Fig. 4f).

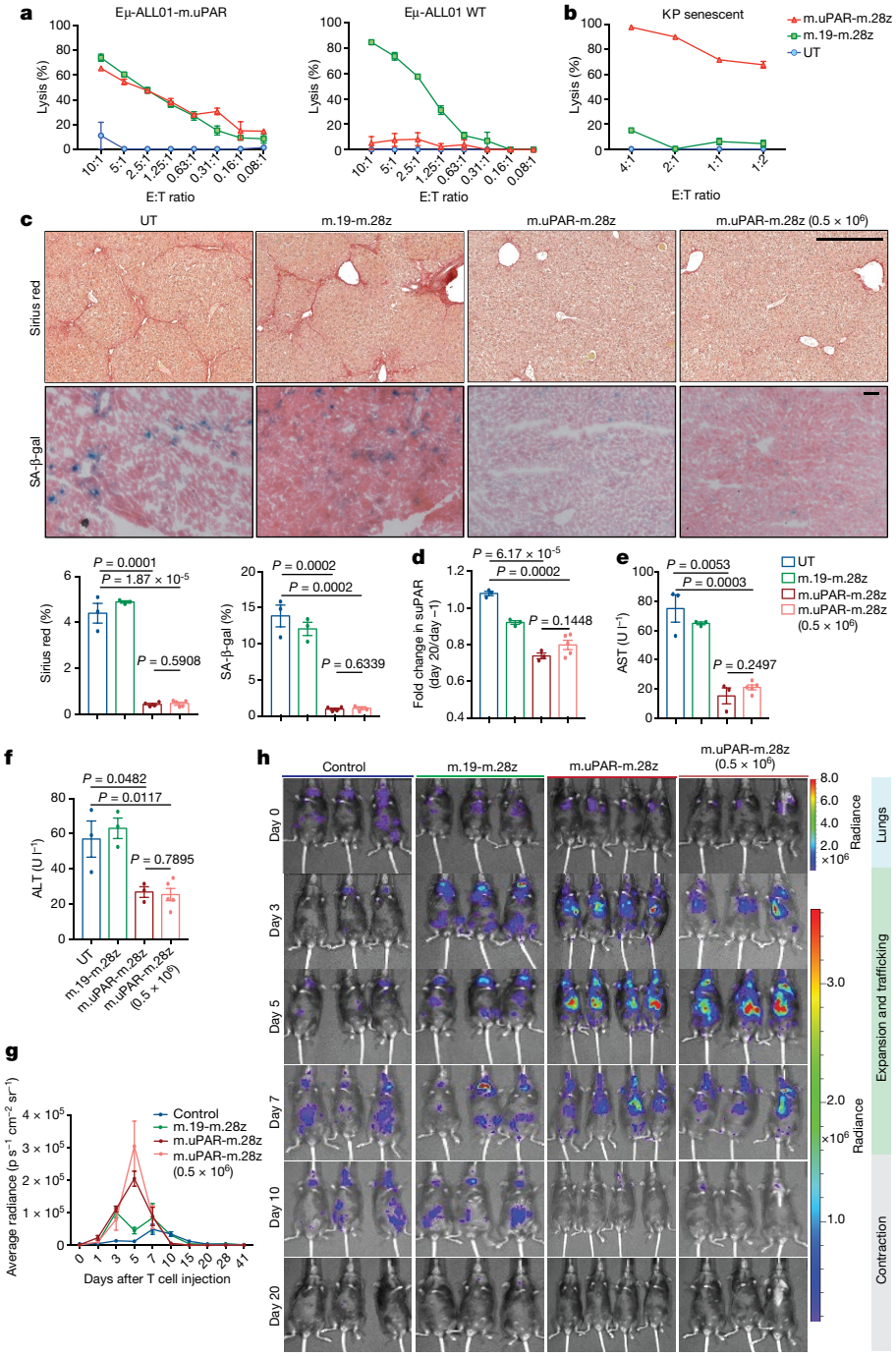

Fig. 3 | Senolytic CAR T cells show therapeutic efficacy in CCl_4-induced liver fibrosis. a, Cytotoxicity of mouse CAR T cells as determined by an 18-h bioluminescence assay using luciferase-expressing wild-type Eμ-ALL01 cells (WT) or Eμ-ALL01 cells that overexpress mouse uPAR (Eμ-ALL01-m.uPAR) as targets. Data are representative of $n = 3$ independent experiments, each performed in triplicate. **b**, Cytotoxic T cell activity as determined by an 18-h bioluminescence assay using KP cells as targets in which senescence was induced by MEK and CDK4/6 inhibition. Data are representative of $n = 2$ independent experiments, each performed in triplicate. **c**–**f**, Mice with CCl_4-induced liver fibrosis were treated with 0.5×10^6 or 1×10^6 m.uPAR-m.28z CAR T cells, 1×10^6 m.19-m.28z CAR T cells or untransduced T cells and euthanized 20 days later. Livers were used for further analyses. **c**, Representative levels of fibrosis as evaluated by Sirius red staining and SA-β-gal expression (top) and respective quantifications (bottom) (UT and m.19-m.28z, $n = 3$; m.uPAR-m.28z, $n = 4$; m.uPAR-m.28z at 0.5×10^6, $n = 5$ mice). Scale bars, 500 μm (top); 50 μm (bottom). **d**, Fold change difference in the serum levels of suPAR 20 days after (day 20) compared to 1 day before (day −1) infusion of T cells. **e**, **f**, Levels of serum AST (**e**) and ALT (**f**) 20 days after infusion of T cells (UT, m.19-m.28z and m.uPAR-m.28z, $n = 3$; m.uPAR-m.28z at 0.5×10^6, $n = 5$ mice (**d**–**f**)). **g**, **h**, Mice with CCl_4-induced liver fibrosis were injected with 0.5×10^6 or 1×10^6 m.uPAR-m.28z CAR T cells, 1×10^6 m.19-m.28z CAR T cells or control T cells that were transduced to express click beetle red luciferase. **g**, Luciferase signal (average radiance) of treated mice after administration of T cells, reflecting the expansion of T cells (control T cells and m.19-m.28z, $n = 3$; m.uPAR-m.28z, $n = 4$; m.uPAR-m.28z at 0.5×10^6, $n = 3$ mice). **h**, Representative bioluminescence images of mice at different time points after injection. T cells were initially detected in the lungs in all treated mice; m.uPAR-m.28z CAR T cells showed trafficking to the liver area followed by a short period of expansion and a rapid contraction. The signal in control mice at day 10 indicates abdominal peritonitis induced by CCl_4 injections, as confirmed by pathology. For the colour scales on the right (measured in p s^{-1} cm^{-2} sr^{-1}), the minimum value and maximum values are 1.43×10^4 and 8.00×10^6, respectively (top) and 1.50×10^5 and 3.63×10^6, respectively (bottom). Results of $n = 1$ independent experiment (**c**–**h**). Data are mean ± s.e.m.; two-tailed unpaired Student's *t*-test (**c**–**f**).

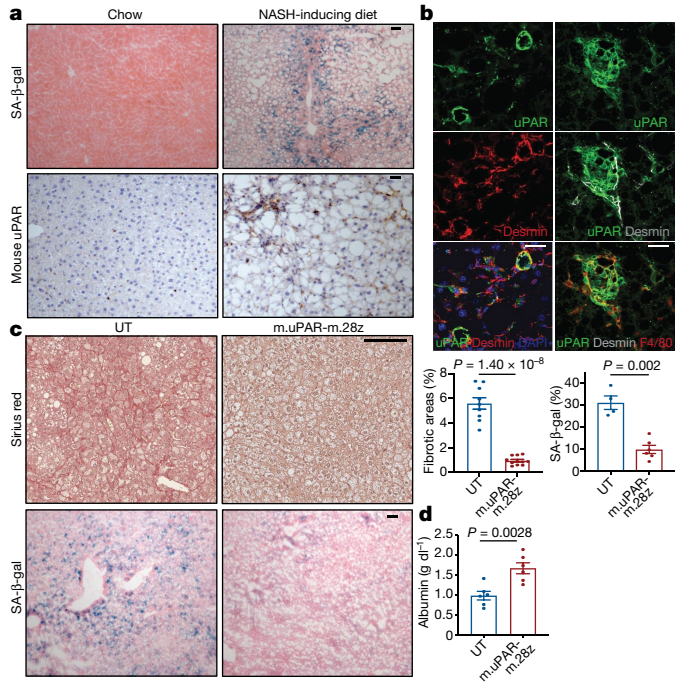

Fig. 4 | Senolytic CAR T cells are therapeutic in NASH-induced liver fibrosis. **a**, **b**, Representative staining in the livers of mice that were treated with a chow or a NASH-inducing diet for 3–4 months. **a**, Immunohistochemical staining of mouse uPAR and SA-β-gal. Scale bars, 50 µm. **b**, Co-immunofluorescence staining of mouse uPAR (green), desmin (red, left; or grey, right) and F4/80 (red) in livers of mice treated with NASH-inducing diet for 3–4 months. Representative results of $n = 2$ independent experiments ($n = 3$ mice per group). Scale bars, 30 µm. **c**, **d**, Mice that were treated with a NASH-inducing diet for 3 months were injected with 0.5×10^6 m.uPAR-m.28z CAR T cells or untransduced T cells. Liver and serum analyses were performed 20 days later. **c**, Representative images of Sirius red staining and SA-β-gal expression (left) and quantifications (right) (Sirius red: UT, $n = 9$; m.uPAR-m.28z, $n = 11$; SA-β-gal: UT, $n = 4$; m.uPAR-m.28z, $n = 6$ mice). Scale bars, 200 µm (top); 50 µm (bottom). **d**, Serum albumin levels (UT and m.uPAR-m.28z, $n = 6$ mice). Results of $n = 2$ independent experiments (**c**, **d**). Data are mean ± s.e.m.; two-tailed unpaired Student's *t*-test (**c**, **d**).

Treatment with m.uPAR-h.28z CAR T cells led to a profound decrease in the bioluminescence signal within 10 days (Fig. 2c), suggesting effective clearance of senescent hepatocytes. Histological analyses confirmed that livers from mice that were treated with m.uPAR-h.28z CAR T cells had significantly reduced numbers of NRAS-positive cells ($P < 0.01$) and SA-β-gal-positive cells ($P < 0.001$) compared to livers from control mice (Fig. 2d, e). Furthermore, m.uPAR-h.28z CAR T cells (but not untransduced T cells) accumulated around senescent hepatocytes within 7 days of infusion (Fig. 2f) and displayed an effector memory phenotype ($CD62L^-CD45RA^-$) with little evidence of T cell exhaustion (less than 2% $PD\text{-}1^+TIM3^+LAG3^+$ CAR T cells) 15 days after their administration (Fig. 2g–i, Extended Data Fig. 11). Therefore, uPAR-28z CAR T cells can eliminate senescent cells in vivo.

Efficacy of senolytic CAR T cells

To evaluate the senolytic capacity of uPAR CAR T cells in immunocompetent settings, we transduced T cells from C57BL/6 mice with a fully mouse CAR (m.uPAR-m.28z). We confirmed CAR expression and excluded uPAR expression on transduced T cells, and showed that they exhibited a similar cytolytic profile to m.uPAR-h.28z CAR T cells when targeting the mouse $CD19^+$ B-ALL cell line Eμ-ALL01 genetically modified to express exogenous uPAR or when targeting senescent KP cells (Fig. 3a, b, Extended Data Fig. 4g, h).

Previous studies suggest that the combination of a senescence-inducing cancer therapy and a senolytic agent can improve treatment outcome in mouse models[30]. We thus treated mice that had orthotopic KP lung adenocarcinomas with combined MEK and CDK4/6 inhibitors[19], and then administered uPAR- or CD19-specific CAR T cells or untransduced T cells (Extended Data Fig. 5a). Treatment with uPAR-targeted CAR T cells significantly prolonged survival without eliciting signs of toxicity (Extended Data Fig. 5b–d). Lungs that were collected from mice treated with uPAR-specific CAR T cells showed a substantial decrease in senescent tumour cells, accompanied by enhanced infiltration of adoptively transferred $CD4^+$ and $CD8^+$ T cells that expressed activation markers (Extended Data Fig. 5e, f). In addition to confirming the senolytic properties of uPAR-directed CAR T cells, these results indicate that combinatorial strategies using senolytic CAR T cells could be used to treat solid tumours.

Besides cancer, senescence contributes to a range of chronic tissue pathologies, including liver fibrosis—a condition that can evolve into cirrhosis and produces a microenvironment that favours the development of hepatocellular carcinoma[1,2]. As genetic ablation of senescent cells ameliorates liver fibrosis[31,32], we performed dose-escalation studies using m.uPAR-m.28z CAR T cells in the well-defined mouse model of CCl_4-induced liver fibrosis, in which treatment with CCl_4 leads to the accumulation of senescent HSCs, fibrosis and liver damage within six weeks[6]. m.uPAR-m.28z CAR T cells, m.19-m.28z CAR T cells or untransduced T cells were infused at either the previously effective dose of $0.5–1 \times 10^6$ CAR T cells or a higher dosage ($2–3 \times 10^6$) into mice with established liver fibrosis[33] (Extended Data Fig. 6a). In some experiments, mice were treated with m.uPAR-m.28z, m.19-m.28z or control T cells that express click beetle red luciferase to track T cells in vivo using bioluminescence[34] (Extended Data Fig. 6b).

At either dosage, treatment with m.uPAR-m.28z CAR T cells produced a marked reduction in liver fibrosis compared to treatment with m.19-m.28z or untransduced T cells. Hence, liver samples obtained from mice 20 days after treatment with m.uPAR-m.28z CAR T cells had fewer senescent cells and less fibrosis (as assessed by SA-β-gal and Sirius red staining) than controls ($P < 0.001$), and this was associated with an accumulation of adoptively transferred T cells (Fig. 3c, Extended Data Fig. 6c, d). Consistent with on-target activity and a therapeutic benefit, mice that were treated with m.uPAR-m.28z CAR T cells showed reduced serum levels of suPAR and of the liver enzymes alanine aminotransferase (ALT) and aspartate aminotransferase (AST) (Fig. 3d–f, Extended Data Fig. 6e–g), indicating efficient elimination of pro-inflammatory senescent HSCs[31,32] and a reduction in liver damage, respectively. Bioluminescence imaging revealed that transferred T cells at first transited through the lungs as expected. Eventually, uPAR-specific CAR T cells—but not CD19-directed CAR T cells or untransduced T cells—accumulated in the livers of CCl_4-treated mice, showing expansion over a few days followed by rapid contraction (Fig. 3g, h). The high senolytic activity of uPAR CAR T cells was corroborated by an efficient reduction of fibrosis under the aggravated conditions produced by prolonged exposure to CCl_4, as well as a sustained resolution of fibrosis in long-term follow-up studies (Extended Data Fig. 6h, i).

Mice treated at the lower effective dose remained highly active and did not display observable signs of morbidity, changes in temperature or weight or relevant alterations in cell blood counts (Extended Data Fig. 7a–c, e). A moderate infiltration of macrophages was noted in the lungs after 20 days, which also occurred in mice treated with m.19-m.28z CAR T cells or untransduced T cells (Extended Data Fig. 7d). Mice treated at the supratherapeutic dose presented with hypothermia and weight loss, which was accompanied by a rise in serum cytokines including IL-6, GM-CSF, G-CSF and IFNγ (Extended Data Fig. 8a–e). Similar to CAR T cell-associated cytokine-release syndrome (CRS)[35,36], this early toxicity was transient, associated with local accumulation and activation of macrophages and could be mitigated by lower doses of CAR T cells or treatment with CRS-preventing inhibitors of IL-6R and IL-1R (Extended Data

Figs. 8f–i, 9). Altogether, these findings indicate that uPAR-directed CAR T cells at an appropriate dosage can deplete senescent cells without inducing severe CRS-like symptoms, and highlight the potential of short-acting CD28- and CD3ζ-based CAR T cells[37] in senescence-associated indications.

We also tested whether CAR T cells that target uPAR could be effective against fibrosis induced by non-alcoholic steatohepatitis (NASH)—a condition that is increasing in incidence and for which effective therapeutic options are lacking[38]. Although the contribution of cellular senescence to the pathology of NASH is poorly understood, its role in other fibrosis settings prompted us to test two well-established mouse models of NASH for the presence of senescent cells. Indeed, senescent cells were prevalent around the fibrotic areas (Fig. 4a, Extended Data Fig. 10a) and co-expressed uPAR together with either a marker of HSCs (desmin) or a marker of macrophages (F4/80) (Fig. 4b). Accordingly, treatment of mice with diet-induced NASH using 0.5×10^6 m.uPAR-m.28z CAR T cells—but not untransduced control T cells—efficiently eliminated senescent cells, reduced fibrosis and improved liver function (as assessed by serum albumin levels) without eliciting detectable toxicity (Fig. 4c, d, Extended Data Fig. 10b–f). Thus, senolytic CAR T cells are effective against liver fibrosis of different aetiologies.

Perspectives

Here we identify uPAR as a protein that is broadly induced on the surface of senescent cells, and we show that uPAR-targeted CAR T cells can eliminate senescent cells in vitro and in vivo. Owing to its secretion, suPAR serves as a plasma biomarker to assess the senolytic activity of CAR T cells in vivo. Whereas a previous report investigated uPAR as a CAR target in ovarian cancer[39], our results provide proof-of-principle of the therapeutic potential of senolytic CAR T cells in senescence-associated pathologies. Although further work is needed to determine whether uPAR-targeting CAR T cells have the required safety profile to be developed clinically, appropriately dosed senolytic CAR T cells can infiltrate the areas of senescence, efficiently target senescent cells and produce a therapeutic benefit without notable toxicity in mice. Future iterations of this approach could target other cell-surface molecules that are specific to particular senescence contexts, incorporate safety switches[40,41] or use combinatorial strategies to maximize efficacy while minimizing side-effects[14,41].

Unlike tumour cells, senescent cells do not divide or create an immunosuppressive microenvironment, and may present fewer barriers to the development of therapeutically efficacious CAR T cells[18,42]. Furthermore, the rapid waning of senolytic CAR T cells used in our studies soon after their therapeutic action may prove an attractive feature in reducing their potential interference with beneficial aspects of senescence and enabling readministration at later times. Beyond fibrosis, senescence has been linked to many disorders of chronic tissue damage that are associated with ageing, such as severe atherosclerosis, diabetes and osteoarthritis[10]. Consequently, senolytic CAR T cells may have broad therapeutic potential.

Online content

Any methods, additional references, Nature Research reporting summaries, source data, extended data, supplementary information, acknowledgements, peer review information; details of author contributions and competing interests; and statements of data and code availability are available at https://doi.org/10.1038/s41586-020-2403-9.

1. He, S. & Sharpless, N. E. Senescence in health and disease. *Cell* **169**, 1000–1011 (2017).
2. Sharpless, N. E. & Sherr, C. J. Forging a signature of in vivo senescence. *Nat. Rev. Cancer* **15**, 397–408 (2015).
3. Serrano, M., Lin, A. W., McCurrach, M. E., Beach, D. & Lowe, S. W. Oncogenic *ras* provokes premature cell senescence associated with accumulation of p53 and $p16^{INK4a}$. *Cell* **88**, 593–602 (1997).
4. Kang, T. W. et al. Senescence surveillance of pre-malignant hepatocytes limits liver cancer development. *Nature* **479**, 547–551 (2011).
5. Demaria, M. et al. An essential role for senescent cells in optimal wound healing through secretion of PDGF-AA. *Dev. Cell* **31**, 722–733 (2014).
6. Krizhanovsky, V. et al. Senescence of activated stellate cells limits liver fibrosis. *Cell* **134**, 657–667 (2008).
7. Collado, M., Blasco, M. A. & Serrano, M. Cellular senescence in cancer and aging. *Cell* **130**, 223–233 (2007).
8. Baker, D. J. et al. Clearance of $p16^{Ink4a}$-positive senescent cells delays ageing-associated disorders. *Nature* **479**, 232–236 (2011).
9. Baar, M. P. et al. Targeted apoptosis of senescent cells restores tissue homeostasis in response to chemotoxicity and aging. *Cell* **169**, 132–147 (2017).
10. Childs, B. G. et al. Senescent intimal foam cells are deleterious at all stages of atherosclerosis. *Science* **354**, 472–477 (2016).
11. Smith, H. W. & Marshall, C. J. Regulation of cell signalling by uPAR. *Nat. Rev. Mol. Cell Biol.* **11**, 23–36 (2010).
12. Kirkland, J. L. & Tchkonia, T. Cellular senescence: a translational perspective. *EBioMedicine* **21**, 21–28 (2017).
13. Xu, M. et al. Senolytics improve physical function and increase lifespan in old age. *Nat. Med.* **24**, 1246–1256 (2018).
14. Sadelain, M., Rivière, I. & Riddell, S. Therapeutic T cell engineering. *Nature* **545**, 423–431 (2017).
15. Park, J. H. et al. Long-term follow-up of CD19 CAR therapy in acute lymphoblastic leukemia. *N. Engl. J. Med.* **378**, 449–459 (2018).
16. Aghajanian, H. et al. Targeting cardiac fibrosis with engineered T cells. *Nature* (2019).
17. Du, H. et al. Antitumor responses in the absence of toxicity in solid tumors by targeting B7-H3 via chimeric antigen receptor T cells. *Cancer Cell* **35**, 221–237 (2019).
18. Pellegatta, S. et al. Constitutive and TNFα-inducible expression of chondroitin sulfate proteoglycan 4 in glioblastoma and neurospheres: implications for CAR-T cell therapy. *Sci. Transl. Med.* **10**, eaao2731 (2018).
19. Ruscetti, M. et al. NK cell-mediated cytotoxicity contributes to tumor control by a cytostatic drug combination. *Science* **362**, 1416–1422 (2018).
20. Perna, F. et al. Integrating proteomics and transcriptomics for systematic combinatorial chimeric antigen receptor therapy of AML. *Cancer Cell* **32**, 506–519 (2017).
21. Tasdemir, N. et al. BRD4 connects enhancer remodeling to senescence immune surveillance. *Cancer Discov.* **6**, 612–629 (2016).
22. Simon, D. I. et al. Mac-1 (CD11b/CD18) and the urokinase receptor (CD87) form a functional unit on monocytic cells. *Blood* **88**, 3185–3194 (1996).
23. Bugge, T. H. et al. The receptor for urokinase-type plasminogen activator is not essential for mouse development or fertility. *J. Biol. Chem.* **270**, 16886–16894 (1995).
24. Coppé, J. P. et al. Senescence-associated secretory phenotypes reveal cell-nonautonomous functions of oncogenic RAS and the p53 tumor suppressor. *PLoS Biol.* **6**, 2853–2868 (2008).
25. Hayek, S. S. et al. Soluble urokinase receptor and chronic kidney disease. *N. Engl. J. Med.* **373**, 1916–1925 (2015).
26. Belcher, C., Fawthrop, F., Bunning, R. & Doherty, M. Plasminogen activators and their inhibitors in synovial fluids from normal, osteoarthritis, and rheumatoid arthritis knees. *Ann. Rheum. Dis.* **55**, 230–236 (1996).
27. Guthoff, M. et al. Soluble urokinase receptor (suPAR) predicts microalbuminuria in patients at risk for type 2 diabetes mellitus. *Sci. Rep.* **7**, 40627 (2017).
28. Schuliga, M. et al. The fibrogenic actions of lung fibroblast-derived urokinase: a potential drug target in IPF. *Sci. Rep.* **7**, 41770 (2017).
29. Brentjens, R. J. et al. Eradication of systemic B-cell tumors by genetically targeted human T lymphocytes co-stimulated by CD80 and interleukin-15. *Nat. Med.* **9**, 279–286 (2003).
30. Wang, C. et al. Inducing and exploiting vulnerabilities for the treatment of liver cancer. *Nature* **574**, 268–272 (2019).
31. Schnabl, B., Purbeck, C. A., Choi, Y. H., Hagedorn, C. H. & Brenner, D. Replicative senescence of activated human hepatic stellate cells is accompanied by a pronounced inflammatory but less fibrogenic phenotype. *Hepatology* **37**, 653–664 (2003).
32. Puche, J. E. et al. A novel murine model to deplete hepatic stellate cells uncovers their role in amplifying liver damage in mice. *Hepatology* **57**, 339–350 (2013).
33. Kuhn, N. F. et al. CD40 ligand-modified chimeric antigen receptor T cells enhance antitumor function by eliciting an endogenous antitumor response. *Cancer Cell* **35**, 473–488 (2019).
34. Dobrenkov, K. et al. Monitoring the efficacy of adoptively transferred prostate cancer-targeted human T lymphocytes with PET and bioluminescence imaging. *J. Nucl. Med.* **49**, 1162–1170 (2008).
35. Giavridis, T. et al. CAR T cell-induced cytokine release syndrome is mediated by macrophages and abated by IL-1 blockade. *Nat. Med.* **24**, 731–738 (2018).
36. Norelli, M. et al. Monocyte-derived IL-1 and IL-6 are differentially required for cytokine-release syndrome and neurotoxicity due to CAR T cells. *Nat. Med.* **24**, 739–748 (2018).
37. Feucht, J. et al. Calibration of CAR activation potential directs alternative T cell fates and therapeutic potency. *Nat. Med.* **25**, 82–88 (2019).
38. Brunt, E. M. et al. Nonalcoholic fatty liver disease. *Nat. Rev. Dis. Primers* **1**, 15080 (2015).
39. Wang, L. et al. Basing on uPAR-binding fragment to design chimeric antigen receptors triggers antitumor efficacy against uPAR expressing ovarian cancer cells. *Biomed. Pharmacother.* **117**, 109173 (2019).
40. Paszkiewicz, P. J. et al. Targeted antibody-mediated depletion of murine CD19 CAR T cells permanently reverses B cell aplasia. *J. Clin. Invest.* **126**, 4262–4272 (2016).
41. Gargett, T. & Brown, M. P. The inducible caspase-9 suicide gene system as a "safety switch" to limit on-target, off-tumor toxicities of chimeric antigen receptor T cells. *Front. Pharmacol.* **5**, 235 (2014).
42. Anderson, K. G., Stromnes, I. M. & Greenberg, P. D. Obstacles posed by the tumor microenvironment to T cell activity: a case for synergistic therapies. *Cancer Cell* **31**, 311–325 (2017).

Methods

RNA extraction, RNA-seq library preparation and sequencing

Total RNA was isolated from three different models of senescence. (1) *Kras*^{G12D}*;p53*$^{-/-}$ cells after 8 days of treatment with vehicle (dimethyl sulfoxide (DMSO)) or combined treatment with the MEK inhibitor trametinib (25 nM) and the CDK4/6 inhibitor palbociclib (500 nM). (2) Oncogene-induced senescent hepatocytes generated in C57BL/6 mice by HTVI. For each mouse, 25 μg of pT3-EF1a-Nras^{G12V}-IRES-GFP-P2A-luciferase plasmid (or pT3-EF1a-Nras$^{G12V;D38A}$-IRES-GFP-P2A-luciferase plasmid as control) and 5 μg CMV-SB13 were suspended in saline solution at the volume of 10% of mouse body weight for administration. Six days after HTVI, mice were anaesthetized and placed on the platform for liver perfusion. Sequential perfusions of Hank's balanced salt solution (HBSS) containing EGTA and HBSS containing collagenase IV were performed, followed by passing the dissociated liver cells through a 100-μm cell strainer. The hepatocytes were then washed again using low-glucose Dulbecco's modified Eagle's medium (DMEM) and centrifuged at a low speed. DAPI-negative and GFP-positive hepatocytes, indicating successful transduction of mutant *Nras* expression, were isolated through low-pressure fluorescence-activated cell sorting (FACS). 3) Senescent or proliferating HSCs (datasets were obtained from a previous study[43]) and proliferating, quiescent or senescent IMR-90 cells (datasets were obtained from a previous study[21]). Sequencing and library preparation were performed at the Integrated Genomics Operation (IGO) at the Memorial Sloan Kettering Cancer Center (MSKCC). RNA-seq libraries were prepared from total RNA. After RiboGreen quantification and quality control by Agilent BioAnalyzer, 100–500 ng of total RNA underwent poly(A) selection and TruSeq library preparation according to the instructions provided by Illumina (TruSeq Stranded mRNA LT Kit, RS-122-2102), with 8 cycles of PCR. Samples were barcoded and run on a HiSeq 4000 or HiSeq 2500 in a 50 bp–50 bp paired-end run, using the HiSeq 3000/4000 SBS Kit or TruSeq SBS Kit v.4 (Illumina) at MSKCC's IGO core facility.

RNA-seq read mapping, differential gene expression analysis and heat map visualization

The resulting RNA-seq data were analysed by removing adaptor sequences using Trimmomatic[44]. RNA-seq reads were then aligned to GRCm38.91 (mm10) with STAR[45] and the transcript count was quantified using featureCounts[46] to generate a raw-count matrix. Differential gene expression analysis and adjustment for multiple comparisons were performed using the DESeq2 package[47] between experimental conditions, with two independent biological replicates per condition, implemented in R (http://cran.r-project.org/). Genes were determined to be differentially expressed on the basis of a greater than two-fold change in gene expression with an adjusted *P* value of less than 0.05. For heat map visualization of differentially expressed genes, samples were normalized by *z*-score and plotted using the pheatmap package in R. Transcripts encoding molecules that were determined to be located in the plasma membrane with a confidence score higher than 3 (range 0–5) as determined by UniProtKB were considered cell-surface molecules.

Functional annotations of gene clusters

Pathway enrichment analysis was performed in the resulting gene clusters with the Reactome database using Enrichr[48]. The significance of the tests was assessed using a combined score, described as $c = \log(p) \times z$, in which c is the combined score, p is the Fisher's exact test P value and z is the z-score for deviation from expected rank.

Cell lines and compounds

The following cell lines were used in this study: mouse *Kras*$^{G12D/+}$*;Trp53*$^{-/-}$ (KP) lung cancer cells (provided by T. Jacks and expressing luciferase–GFP as described[19]), and NALM6 and Eμ-ALL01 cells expressing firefly luciferase–GFP[37]. Cells were maintained in a humidified incubator at 37 °C with 5% CO_2. KP cells were grown in DMEM supplemented with 10% fetal bovine serum (FBS) and 100 IU ml^{-1} penicillin–streptomycin. NALM6 and Eμ-ALL01 cells were grown in complete medium composed of RPMI supplemented with 10% FBS, 1% L-glutamine, 1% MEM non-essential amino acids, 1% HEPES buffer, 1% sodium pyruvate, 0.1% β-mercaptoethanol and 100 UI ml^{-1} penicillin–streptomycin. Human primary melanocytes were grown in dermal cell basal medium (ATCC, 200-030) supplemented with the adult melanocyte growth kit (ATCC, 200-042), 10% FBS and 100 IU ml^{-1} penicillin–streptomycin. All cell lines used were negative for mycoplasma.

For drug-induced senescence experiments in vitro, trametinib (S2673) and palbociclib (S1116) were purchased from Selleck Chemicals and dissolved in DMSO to yield 10 mM stock solutions, which were stored at −80 °C[19]. Cells were treated with MEK inhibitor (25 nM) and CDK4/6 inhibitor (500 nM). The growth medium was changed every two days. For in vivo experiments trametinib was dissolved in a 5% hydroxypropyl methylcellulose and 2% Tween-80 solution (Sigma) and palbociclib was dissolved in sodium lactate buffer (pH 4) (as described previously[19]). Mice were treated with 1 mg per kg body weight of trametinib and 150 mg per kg body weight of palbociclib as previously described[19]. Caerulein was purchased from Bachem. Anakinra was purchased from Sobi and administered intraperitoneally at a dose of 30 mg per kg body weight twice a day for 8 days starting 24 h before transfer of CAR T cells. Anti-mouse IL-6R (clone MP5-20F3) was purchased from BioXCell and administered intraperitoneally once per day at 25 mg per kg body weight for the first dose and 12.5 mg per kg body weight for subsequent doses for 8 days starting 24 h before transfer of CAR T cells as previously described[35].

SA-β-gal staining

SA-β-gal staining was performed as previously described[19] at pH 6.0 for human cells and tissue and pH 5.5 for mouse cells and tissue. Fresh frozen tissue sections or adherent cells plated in 6-well plates were fixed with 0.5% glutaraldehyde in phosphate-buffered saline (PBS) for 15 min, washed with PBS supplemented with 1 mM $MgCl_2$ and stained for 5–8 h in PBS containing 1 mM $MgCl_2$, 1mg ml^{-1} X-gal, 5 mM potassium ferricyanide and 5 mM potassium ferrocyanide. Tissue sections were counterstained with eosin. Five high power fields per well or section were counted and averaged to quantify the percentage of SA-β-gal$^+$ cells.

Quantitative PCR with reverse transcription

Total RNA was isolated using the RNeasy Mini Kit (Qiagen) and cDNA was obtained using TaqMan reverse-transcription reagents (Applied Biosystems). Quantitative PCR (qPCR) was performed in triplicates using SYBR green PCR master mix (Applied Biosystems) on the ViiA 7 Real-Time PCR System (Invitrogen). *GAPDH* or *ACTB* served as endogenous normalization controls for mouse and human samples.

Mice

All mouse experiments were approved by the MSKCC Internal Animal Care and Use Committee. All relevant animal use guidelines and ethical regulations were followed. Mice were maintained under specific pathogen-free conditions, and food and water were provided ad libitum. The following mice were used: C57BL/6N background, NOD-scid IL2Rg^{null} (NSG) mice (purchased from The Jackson laboratory) and B6.SJL-Ptrc^a/BoyAiTac (CD45.1 mice) (purchased from Taconic). Mice of both sexes were used at 8–12 weeks of age (5–7 weeks old for the xenograft experiments and 6–10 weeks old for T cell isolation) and were kept in group housing. Mice were randomly assigned to the experimental groups.

Transposon-mediated intrahepatic gene transfer

Transposon-mediated intrahepatic gene transfer was performed as previously described[4]. In brief, 8–12-week-old C57BL/6J mice received a saline solution at a final volume of 10% of their body weight containing 30 μg of total DNA composed of a 5:1 molar ratio of transposon-encoding

vector (containing either the sequence for $Nras^{G12V}$ or the sequence for the GTPase-dead form $Nras^{G12V/D38A}$) to transposase-encoding vector (*Sleeping Beauty* 13) through HTVI. For CAR T cell studies, NSG mice were intravenously injected with 0.5×10^6 human CAR T cells or untransduced T cells 10 days after HTVI and monitored by bioluminescence imaging using the IVIS Imaging System (PerkinElmer) with Living Image software (PerkinElmer). At day 15 after CAR injection, mice were euthanized and livers were removed and used for further analysis.

Generation of mouse pancreatic intraepithelial neoplasias

The mouse strain has been previously described[49]. To induce pancreatic intraepithelial neoplasias, KC;RIK (p48-Cre;RIK;LSLKrasG12D) male mice were treated with eight (one per hour) intraperitoneal injections of 80 μg kg^{-1} caerulein (Bachem) for two consecutive days. Mice were then euthanized 21 weeks later and their pancreases were used for further analysis. Age-matched C;RIK mice (expressing wild-type *Kras*) injected with PBS were used as controls for normal pancreas.

In vivo induction of CCl_4-induced liver fibrosis

C57BL/6N mice were treated twice a week with 12 consecutive intraperitoneal injections of 1 ml kg^{-1} tetrachloride (CCl_4) to induce liver fibrosis[6,43]. For mouse CAR T cell studies, cyclophosphamide (200 mg kg^{-1}) was administered 16–24 h before T cell injection. Mice received $0.5–1 \times 10^6$ or $2–3 \times 10^6$ CAR T cells or untransduced T cells (same total numbers of T cells) and CCl_4 was continuously administered at the same dose and interval until day 20 after CAR T cell injection, when mice were euthanized 48–72 h after the last CCl_4 injection. Blood was collected by facial vein puncture or cardiac puncture.

In vivo induction of NASH-induced liver fibrosis

C57BL/6N mice were fed with a NASH-inducing diet (Teklad TD.160785, which contains 10.2% kcal from protein, 37.3% kcal from carbohydrate and 52.6% kcal from fat) and fructose-containing drinking water (23.1 g fructose and 18.9 g glucose dissolved in 1 l water and then filter-sterilized) at 8–10 weeks of age[50,51]. Body weight was measured weekly. For mouse CAR T cell studies, cyclophosphamide (200 mg kg^{-1}) was administered 16 h before T cell injection. Mice received 0.5×10^6 CAR T cells or untransduced T cells (same total numbers of T cells) and they received the same NASH diet until day 20 after T cell injection, when they were euthanized. Blood was collected by facial vein puncture or cardiac puncture.

For the 'STAM' model[52], liver tissue samples (unstained slides for immunohistochemistry) were purchased from SMC laboratories.

Patient-derived xenografts

Experiments with patient-derived xenografts were performed as described[19], using 5–7-week-old female NSG mice. MSK-LX27 was derived from a lung adenocarcinoma containing $KRAS^{G12D}$ and *P53* (*P53* is also known as *TP53*) mutations and a deletion in *CDKN2A* and was cut into pieces and inserted in the subcutaneous space. Mice were monitored daily, weighed twice weekly and caliper measurements began when tumours became visible. Tumours were measured using the formula: tumour volume = $(D \times d^2)/2$ (in which D is the longer diameter and d is the shorter diameter) and when they reached a size of 100–200 mm^3, mice were randomized on the basis of the starting tumour volume and treated with vehicle or trametinib (3 mg per kg body weight) and palbociclib (150 mg per kg body weight) orally for 4 consecutive days followed by 3 days off treatment. Experimental end points were achieved when tumours reached a size of 2,000 mm^3 or became ulcerated. Tumours were collected at the experimental end point and tissue was divided evenly for 10% formalin fixation and optimal cutting temperature (OCT) compound frozen blocks.

Patient samples

De-identified human samples from liver biopsies of patients with liver fibrosis from viral (hepatitis B or C), alcoholic and non-alcoholic fatty liver disease were obtained through the Department of Pathology at Mount Sinai Hospital. Human pancreatic intraepithelial neoplasia samples were obtained through the Department of Pathology at MSKCC. Human atherosclerosis samples were obtained through the Department of Pathology at Weill Medical College of Cornell University. All human studies complied with all relevant guidelines and ethical regulations and were approved by the Institutional Review Board at Mount Sinai, Weill Medical College or MSKCC.

Histological analysis

Tissues were fixed overnight in 10% formalin, embedded in paraffin and cut into 5-μm sections. Sections were subjected to haematoxylin and eosin (H&E) staining, and to Sirius red staining for fibrosis detection. For fibrosis quantification, at least three whole sections from each mouse were scanned and the images were quantified using NIH ImageJ software. The amount of fibrotic tissue was calculated relative to the total analysed liver area as previously described. Immunohistochemical and immunofluorescence staining was performed following standard protocols. The following primary antibodies were used: anti-human uPAR (R&D, AF807, lot BBS0318071, 1:50), anti-mouse uPAR (R&D, AF534, lot DCL0418021, 1:50), anti-mouse NRAS (Santa Cruz, SC-31, lot A1020, 1:50), anti-mouse SMA (Abcam, Ab5694, lot GR283004-16, 1:50), anti-mouse KATE (Evrogen, ab233, lot 23301201267, 1:1,000), anti-human CD3 (Abcam, ab5690, lot GR3220039-4, 1:100), Myc-tag (Cell Signaling, 2276S, lot 24, 1:50), anti-mouse Ki-67 (Abcam, ab16667, lot GR3305281-1, 1:200), anti-mouse IL-6 (Abcam, ab6672, lot GR3195128-19, 1:50), p16-INK4A (Proteintech, 10883-1-AP, lot 00057396, 1:50), anti-mouse P-ERKT202/Y204 (Cell Signaling.4370, lot 1:800), desmin (Thermo Fisher Scientific, RB-9014, lot 9014p1806Q, 1:200), AF488 donkey anti-rabbit (Invitrogen, A21206, lot 1874771, 1:500), AF488 donkey anti-mouse (Invitrogen, A21202, lot 1820538, 1:500), AF594 donkey anti-rabbit (Invitrogen, A21207, lot 1602780, 1:500), AF594 donkey anti-mouse (Invitrogen, A21203, lot 1163390, 1:500), AF594 donkey anti-goat (Invitrogen, A11058, lot 2045324, 1:500), AF594 goat anti-rat (Invitrogen, A11007, lot 1903506, 1:500).

Flow cytometry

For analysis of uPAR expression in cell lines after induction of senescence, KP cells were treated with trametinib (25 nM) and palbociclib (500 nM) or with vehicle (DMSO), and human primary melanocytes were continuously passaged for 15 passages and then trypsinized, resuspended in PBS supplemented with 2% FBS and stained with the following antibodies for 30 min on ice: PE-conjugated anti-mouse uPAR (R&D, FAB531P) or APC-conjugated anti-human uPAR (Thermo Fisher Scientific, 17-3879-42). The following fluorophore-conjugated antibodies were used for in vitro and in vivo experiments in the indicated dilutions ('h' prefix denotes anti-human; 'm' prefix denotes anti-mouse): hCD45 APC-Cy7 (clone 2D1, BD, 557833, lot 9081815, 1:100), hCD4 BUV395 (clone SK3, BD, 563550, lot 6252529, 1:100), hCD4 BV480 (clone SK3, BD, 566104, lot 8092993, 1:50), hCD62L BV421 (clone DREG-56, BD, 563862, lot 8194954, 1:100), hCD45RA BV650 (clone HI100, BD, 563963, lot 9057952, 1:100), hPD-1 BV480 (clone EH12.1, BD, 566112, lot 8235507, 1:100), hCD19 BUV737 (clone SJ25C1, BD, 564303, lot 8130572, 1:100), hCD271 PE (clone C40-1457, BD, 557196, lot 7068641, 1:100), hIL-2 PE-Cy7 (clone MQ1-17H12, Invitrogen, 25-7029-42, lot 4336863, 1:50), hTNF BV650 (clone Mab11, BD, 563418, lot 7082880, 1:50), hIFNγ BUV395 (clone B27, BD, 563563, lot 6320836, 1:50) hTIM3 BV785 (clone F38-2E2, Biolegend, 345032, lot B265346, 1:100), hCD8 PE-Cy7 (clone SK1, eBioscience, 25-0087-42, lot 2066348, 1:100), hCD8 APC-Cy7 (clone SK1, BD, 557834, lot 7110951, 1:50), hCD223 PerCP-eFluor710 (clone 3DS223H, eBioscience, 46-2239-42, lot 4321735, 1:100), hGrB APC (clone GB12, Invitrogen, MHGB05, lot 1884625, 1:67), hMyc-tag AF647 (clone 9B11, Cell Signaling Technology, 2233S, lot 23, 1:50), hCD19 PB (clone SJ25-C1, Invitrogen, MHCD1928, 1:100), hCD87 APC (clone VIM5, eBioscience,

17-3879-42, lot 17-3879-42, 1:50), hCD87 PerCp-eFluor710 (clone VIM5, eBioscience, 46-3879-42, lot 46-2239-42, 1:50), muPAR PE (R&D Systems, FAB531P, lot ABLH0419081, 1:50), muPAR AF700 (R&D Systems, FAB531N, lot 1552229, 1:50), mCD45.1 APC-Cy7 (clone A20, Biolegend, 110716, lot B285685, 1:200), m.CD45.1 BV785 (clone A20, Biolegend, 110743, lot B270183, 1:100), mCD45.2 PE (clone 104, Biolegend, 109808, lot B271929, 1:100), mCD45.2 AF700 (clone 104, Biolegend, 109822, lot B252126, 1:200), mSiglec-F PerCP-Cy5.5 (clone E50-2440, BD, 565526, lot 8232650, 1:200), mI-A/I-E BV605 (clone M5/114.15.2, Biolegend, 107639, lot B293222, 1:50), mF4/80 BV421 (clone T45-2342, BD, 565411, lot 8330526, 1:200), mCD11b BUV395 (clone M1/70, BD, 563553, lot 8339988, 1:200), mCD11c BV650 (clone N418, Biolegend, 117339, lot B253523, 1:200), mLY6G BV510 (clone 1A8, Biolegend, 127633, lot B266675, 1:200), mLY6G APC/Fire750 (clone 1A8, Biolegend, 127652, lot B274284, 1:100), miNOS PE-Cy7 (clone CXNFT, eBioscience, 25-5920-82, lot 2127491, 1:200), mCD19 PE (clone 1D3/CD19, Biolegend, 152408, lot B260181, 1:100), mCD25 BV605 (clone PC61, Biolegend, 102035, lot B291215, 1:50), mCD69 PerCpCy5.5 (clone H1.2F3, Biolegend, 104522, lot B244018, 1:100), mCD3 AF488 (clone 17A2, Biolegend, 100210, lot B284975, 1:100), mCD4 BUV395 (clone GK1.5, BD, 563790, lot 9101822, 1:50), mCD4 FITC (clone GK1.5, BD, 553729, lot 9204449, 1:50) and mCD8 PE-Cy7 (Clone: 53-6.7, Biolegend, 100722, lot B282418, 1:50). 7-AAD (BD, 559925, lot 9031655, 1:40), DAPI (Life Technologies D1306), Fixable Viability Dye eFluor 506 (65-0866-14, eBioscience, lot 2095423, 1:200) and LIVE/DEAD Fixable Violet (L34963, Invitrogen, lot 1985351, 1:100) were used as a viability dyes.

CAR staining was performed with Alexa Fluor 647 AffiniPure F(ab')$_2$ Fragment Goat Anti-Rat IgG (Jackson ImmunoResearch, 112-6606-072). For cell counting, CountBright Absolute Counting Beads were added (Invitrogen) according to the manufacturer's instructions. For in vivo experiments, Fc receptors were blocked using FcR blocking reagent, mouse (Miltenyi Biotec). For intracellular cytokine secretion assay, cells were fixed and permeabilized using the Cytofix/Cytoperm Fixation/Permeabilization Solution Kit (BD Biosciences) or Intracellular Fixation & Permeabilization Buffer Set Kit (eBioscience, 88-8824-00) according to the manufacturer's instructions.

Flow cytometry was performed on a LSRFortessa instrument (BD Biosciences) or Cytek Aurora (CYTEK) and data were analysed using FlowJo (TreeStar).

For in vivo sample preparation, livers were dissociated using the MACS liver dissociation kit (Miltenyi Biotec, 130-1-5-807), filtered through a 100-µm strainer and washed with PBS, and red blood cell lysis was achieved with an ACK (ammonium–chloride–potassium) lysing buffer (Lonza). Cells were washed with PBS, resuspended in FACS buffer and used for subsequent analysis. Lungs were minced and digested with 1mg/ml collagenase type IV and DNase type IV in RPMI at 37C and 200rpm for 45 min, filtered through 100µm strainer, washed with PBS, and red blood cell lysis was achieved with an ACK lysing buffer (Lonza). Cells were washed with PBS, resuspended in FACS buffer and used for subsequent analysis. For bone marrow samples, tibias and femurs were mechanically disrupted with a mortar in PBS and 2 mM EDTA, filtered through a 40-µm strainer and washed with PBS and 2 mM EDTA, and red blood cell lysis was achieved with an ACK lysing buffer (Lonza). Cells were washed with PBS and 2 mM EDTA, resuspended in FACS buffer and used for subsequent analysis. Spleens were mechanically disrupted with the back of a 5-ml syringe, filtered through a 40-µm strainer and washed with PBS and 2 mM EDTA and red blood cell lysis was achieved with an ACK lysing buffer (Lonza). Cells were washed with PBS and 2 mM EDTA, resuspended in FACS buffer and used for subsequent analysis.

Cytokine measurements

Serum cytokines were measured using cytometric bead arrays (BD) as per the manufacturer's instructions.

Detection of suPAR levels

suPAR levels from cell culture supernatant or mouse plasma were evaluated by enzyme-linked immunosorbent assay (ELISA) according to the manufacturer's protocol (R&D systems, DY531 (mouse) or DY807 (human)).

Liver function tests

The levels of ALT, AST and albumin in mouse serum were measured according to the manufacturer's protocol, using the EALT-100 (ALT), EASTR-100 (AST) and DIAG-250 (albumin) kits from BioAssay systems.

Isolation, expansion and transduction of human T cells

All blood samples were handled following the required ethical and safety procedures. Peripheral blood was obtained from healthy volunteers and buffy coats from anonymous healthy donors were purchased from the New York Blood Center. Peripheral blood mononuclear cells were isolated by density gradient centrifugation. T cells were purified using the human Pan T Cell Isolation Kit (Miltenyi Biotec), stimulated with CD3/CD28 T cell activator Dynabeads (Invitrogen) as described[37] and cultured in X-VIVO 15 (Lonza) supplemented with 5% human serum (Gemini Bio-Products), 5 ng ml^{-1} interleukin-7 and 5 ng ml^{-1} interleukin-15 (PeproTech). T cells were counted using an automated cell counter (Nexcelom Bioscience).

Forty-eight hours after initiating T cell activation, T cells were transduced with retroviral supernatants by centrifugation on RetroNectin-coated plates (Takara). Transduction efficiencies were determined four days later by flow cytometry and CAR T cells were adoptively transferred into mice or used for in vitro experiments.

Isolation, expansion and transduction of mouse T cells

B6.SJL-Ptrc^{a}/BoyAiTac mice (CD45.1 mice) were euthanized and spleens were collected. After tissue dissection and red blood cell lysis, primary mouse T cells were purified using the mouse Pan T cell Isolation Kit (Miltenyi Biotec). Purified T cells were cultured in RPMI-1640 (Invitrogen) supplemented with 10% FBS (HyClone), 10 mM HEPES (Invitrogen), 2 mM L-glutamine (Invitrogen), MEM non-essential amino acids 1×(Invitrogen), 55 uM β-mercaptoethanol, 1 mM sodium pyruvate (Invitrogen), 100 IU ml^{-1} recombinant human IL-2 (Proleukin; Novartis) and mouse anti-CD3/28 Dynabeads (Gibco) at a bead:cell ratio of 1:2. T cells were spinoculated with retroviral supernatant collected from Phoenix-ECO cells 24 h after initial T cell activation as described[33,53] and used for functional analysis 3–4 days later.

Genetic modification of T cells

The human and mouse SFG γ-retroviral m.uPAR-28z plasmids were constructed by stepwise Gibson assembly (New England BioLabs) using the SFG-1928z backbone as previously described[29,54–56]. The amino acid sequence for the single-chain variable fragment (scFv) specific for mouse uPAR was obtained from the heavy and light chain variable regions of a selective monoclonal antibody against mouse uPAR (R&D MAB531-100) through mass spectometry performed by Bioinformatics Solutions. In the human SFG-m.uPAR-h.28z CARs, the anti-mouse uPAR scFv is thus preceded by a human CD8A leader peptide and followed by CD28 hinge–transmembrane–intracellular regions, and CD3z intracellular domains linked to a P2A sequence to induce co-expression of truncated LNGFR. In the mouse SFG-m.uPAR-m.28z CARs, the anti-mouse uPAR scFv is preceded by a mouse CD8A leader peptide and followed by the Myc-tag sequence (EQKLISEEDL), mouse CD28 transmembrane and intracellular domain and mouse CD3z intracellular domain[33].

Plasmids encoding the SFGγ retroviral vectors were used to transfect gpg29 fibroblasts (H29) to generate VSV-G pseudotyped retroviral supernatants, which were used to construct stable retrovirus-producing cell lines as described[29,33]. For T cell imaging studies, mouse T cells were transduced with retroviral supernatants encoding SFG-GFP-click beetle red luciferase[57].

Cytotoxicity assays

The cytotoxicity of CAR T cells was determined by standard luciferase-based assays or by calcein-AM-based cytotoxicity assays. For luciferase-based assays, target cells expressing firefly luciferase (FFLuc-GFP) were co-cultured with T cells in triplicate at the indicated effector:target ratios using black-walled 96-well plates with 5×10^4 (for NALM6 and Eμ-ALL01) or 1.5×10^4 (for KP) target cells in a total volume of 100 µl per well in RPMI or DMEM medium, respectively. Target cells alone were plated at the same cell density to determine the maximum luciferase expression (relative light units (RLU)) and maximum release was determined by addition of 0.2% Triton-X100 (Sigma). Either 4 or 18 h later, 100 µl luciferase substrate (Bright-Glo, Promega) was directly added to each well. Emitted light was detected in a luminescence plate reader. Lysis was determined as $(1-(RLU_{sample})/(RLU_{max})) \times 100$. For calcein-AM-based assays, target cells (NALM6) were loaded with 20 µM calcein-AM (Thermo Fisher Scientific) for 30 min at 37 °C, washed twice and co-incubated with T cells in triplicate at the indicated effector:target ratios in 96-well round-bottomed plates with 5×10^3 target cells in a total volume of 200 µl per well in complete medium. Target cells alone were plated at the same cell density to determine spontaneous release and maximum release was determined by incubating the targets with 0.2% Triton-X100 (Sigma). After a 4-h co-culture, supernatants were collected and free calcein was quantitated using a Spark plate reader (Tecan). Lysis was calculated as: ((experimental release − spontaneous release)/(maximum release − spontaneous release)) × 100.

Statistical analysis and figure preparation

Data are presented as mean ± s.e.m. Statistical analysis was performed by Student's *t*-test using GraphPad Prism v.6.0 or 7.0 (GraphPad software). *P* values of less than 0.05 were considered to be statistically significant. Survival was determined using the Kaplan–Meier method. No statistical methods were used to predetermine sample size in the mouse studies, and mice were allocated at random to treatment groups. The investigators were not blinded to allocation during experiments and outcome assessment. Figures were prepared using BioRender.com for scientific illustrations and Illustrator CC 2019 (Adobe).

Reporting summary

Further information on research design is available in the Nature Research Reporting Summary linked to this paper.

Data availability

The RNA-seq data have been deposited in the Gene Expression Omnibus under the accession number GSE145642. Source data are provided with this paper. All other data supporting the findings of this study will be made available upon reasonable request to the corresponding authors. Source data

43. Lujambio, A. et al. Non-cell-autonomous tumor suppression by p53. *Cell* **153**, 449–460 (2013).
44. Bolger, A. M., Lohse, M. & Usadel, B. Trimmomatic: a flexible trimmer for Illumina sequence data. *Bioinformatics* **30**, 2114–2120 (2014).
45. Dobin, A. et al. STAR: ultrafast universal RNA-seq aligner. *Bioinformatics* **29**, 15–21 (2013).
46. Liao, Y., Smyth, G. K. & Shi, W. featureCounts: an efficient general purpose program for assigning sequence reads to genomic features. *Bioinformatics* **30**, 923–930 (2014).
47. Love, M. I., Huber, W. & Anders, S. Moderated estimation of fold change and dispersion for RNA-seq data with DESeq2. *Genome Biol.* **15**, 550 (2014).
48. Chen, E. Y. et al. Enrichr: interactive and collaborative HTML5 gene list enrichment analysis tool. *BMC Bioinformatics* **14**, 128 (2013).
49. Livshits, G. et al. Arid1a restrains Kras-dependent changes in acinar cell identity. *eLife* **7**, e35216 (2018).
50. Zhu, C. et al. Hepatocyte Notch activation induces liver fibrosis in nonalcoholic steatohepatitis. *Sci. Transl. Med.* **10**, eaat0344 (2018).
51. Wang, X. et al. Hepatocyte TAZ/WWTR1 promotes inflammation and fibrosis in nonalcoholic steatohepatitis. *Cell Metab.* **24**, 848–862 (2016).
52. Fujii, M. et al. A murine model for non-alcoholic steatohepatitis showing evidence of association between diabetes and hepatocellular carcinoma. *Med. Mol. Morphol.* **46**, 141–152 (2013).
53. Davila, M. L., Kloss, C. C., Gunset, G. & Sadelain, M. CD19 CAR-targeted T cells induce long-term remission and B cell aplasia in an immunocompetent mouse model of B cell acute lymphoblastic leukemia. *PLoS ONE* **8**, e61338 (2013).
54. Maher, J., Brentjens, R. J., Gunset, G., Rivière, I. & Sadelain, M. Human T-lymphocyte cytotoxicity and proliferation directed by a single chimeric TCRζ/CD28 receptor. *Nat. Biotechnol.* **20**, 70–75 (2002).
55. Brentjens, R. J. et al. Genetically targeted T cells eradicate systemic acute lymphoblastic leukemia xenografts. *Clin. Cancer Res.* **13**, 5426–5435 (2007).
56. Hagani, A. B., Rivière, I., Tan, C., Krause, A. & Sadelain, M. Activation conditions determine susceptibility of murine primary T-lymphocytes to retroviral infection. *J. Gene Med.* **1**, 341–351 (1999).
57. Santos, E. B. et al. Sensitive in vivo imaging of T cells using a membrane-bound *Gaussia princeps* luciferase. *Nat. Med.* **15**, 338–344 (2009).
58. Van der Schueren, B. et al. Low cytochrome oxidase 4I1 links mitochondrial dysfunction to obesity and type 2 diabetes in humans and mice. *Int. J. Obes.* **39**, 1254–1263 (2015).

Acknowledgements We thank A. Lujambio and R. Brody and the Biorepository and Pathology Core at Icahn School of Medicine at Mount Sinai, and G. Askan and O. Basturk at the Department of Pathology at MSKCC, for tissue samples; L. Zender and H. Chen for sharing plasmids; N. Salgado, H. Chen, T. Baslan, S. Tian, A. Wuest, W. Luan and G. Gunset for technical assistance; and C. J. Sherr, E. de Stanchina, N. Kuhn, A. Dobrin, M. L. Sjöstrand and other members of the Lowe and Sadelain laboratories for insightful discussions. This work was supported by a grant from the National Institute of Aging (AG065396) to S.W.L., the Pasteur-Weizmann/Servier award to M.S. and a Memorial Sloan Kettering Cancer Center support grant (P30 CA008748) to both S.W.L. and M.S. laboratories. S.L.F. was supported by a grant from the National Institute of Diabetes and Digestive and Kidney Diseases (R01DK56621), a grant from the Department of Defense (CA150272) and the P30 grant (CA165979); C.A. was supported by a postgraduate fellowship from La Caixa foundation and is the recipient of the Harold E. Varmus graduate student fellowship from the Gerstner Sloan Kettering graduate school; J.F. was supported by the Care-for-Rare Foundation and the German Research Foundation (DFG); J.L. was supported by a fellowship from the DFG and a Shulamit Katzman Endowed Postdoctoral Research Fellowship; J.F. and J.L. are part of the Experimental Medicine Program at the University of Tuebingen; D.A.-C. was supported by a postdoctoral fellowship from Fundación Ramón Areces; J.A.B. was supported by the Grayer postgraduate fellowship and the Geoffrey Been graduate student fellowship from the Gerstner Sloan Kettering graduate school; and A.K. was supported by a grant from the National Cancer Institute (U54 0D020355-01). S.W.L. is the Geoffrey Been Chair of Cancer Biology and a Howard Hughes Medical Institute Investigator. We thank the following MSKCC core facilities for support: SKI flow cytometry core facility, animal facility, antitumor assessment core, laboratory for comparative biology, bioinformatics core and integrated genomics operation core.

Author contributions C.A., J.F. and J.L. conceived the project, designed, performed and analysed experiments and wrote the paper with assistance from all authors. Y.-J.H. analysed RNA-seq data. C.Z., D.A.-C., J.M.-S., J.A.B., X.L., A.K., S.H. and T.G. performed and analysed experiments. A.P. performed histopathological toxicity analysis. S.L.F. provided human liver samples, analysed data and reviewed the manuscript. E.P. provided human carotid endarterectomy samples and reviewed the manuscript. V.P. helped with T cell imaging studies. M.S. and S.W.L. conceived the project, supervised experiments and wrote the paper. All authors read and approved of the paper.

Competing interests A patent application (PCT/US2020/016290; filed on 02/01/2020) has been submitted based in part on results presented in this manuscript on the use of CAR T cells that target uPAR as senolytic agents. C.A., J.F., J.L., M.S. and S.W.L. are listed as the inventors. J.F. and M.S. hold other unrelated patents on CAR technologies.S.W.L. is an advisor for and has equity in the following biotechnology companies: ORIC Pharmaceuticals, Faeth Therapeutics, Blueprint Medicines, Geras Bio, Mirimus Inc., PMV Pharmaceuticals and Constellation Pharmaceuticals.

Additional information
Supplementary information is available for this paper at https://doi.org/10.1038/s41586-020-2403-9.
Correspondence and requests for materials should be addressed to M.S. or S.W.L.
Peer review information *Nature* thanks Jesus Gil, Stephen Gottschalk and the other, anonymous, reviewer(s) for their contribution to the peer review of this work.
Reprints and permissions information is available at http://www.nature.com/reprints.

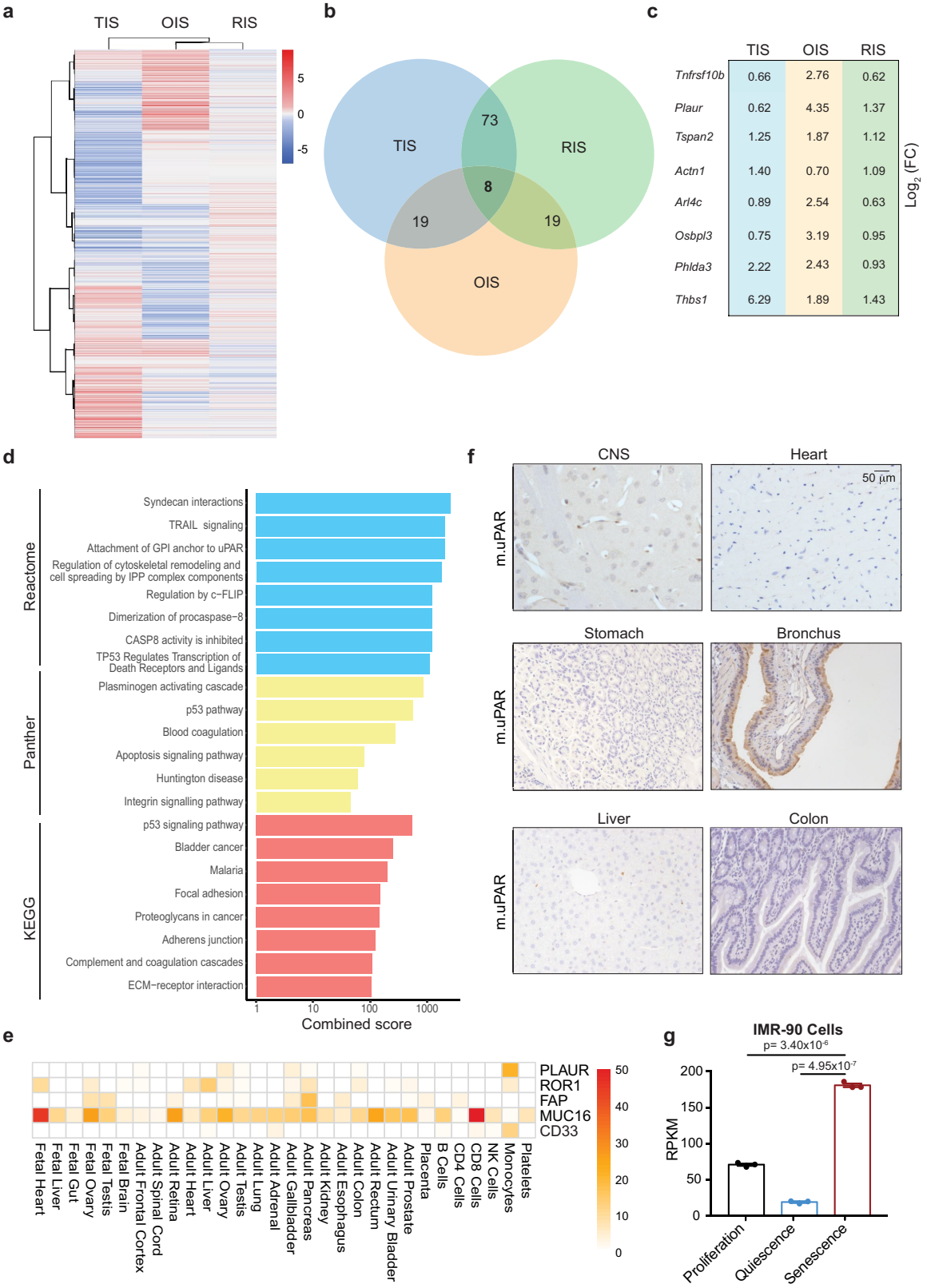

Extended Data Fig. 1 | See next page for caption.

Extended Data Fig. 1 | Genes encoding surface molecules that are commonly upregulated in senescence. a, Heat map of genes upregulated in therapy-induced senescence (TIS), oncogene-induced senescence (OIS) or replication-induced senescence (RIS) in HSCs. **b**, Venn diagram showing the number of common genes upregulated in the three datasets in **a**. **c**, Fold change (log_2(expression in senescent cells/expression in non-senescent cells)) of the eight commonly upregulated genes in the three different datasets in **a**. **d**, Combined enrichment score of significantly enriched gene sets among the eight commonly upregulated genes in senescence. ECM, extracellular matrix; GPI, glycosylphosphatidylinositol. **e**, Heat map showing the expression profile of uPAR (*PLAUR*) in human vital tissues (as determined by the Human Proteome Map) compared to the expression profiles of other targets of CAR T cells in clinical trials. NK cells, natural killer cells. **f**, Immunohistochemical staining of mouse uPAR (m.uPAR) in vital tissues of C57BL/6J mice. Representative results of $n = 2$ independent experiments. **g**, Reads per kilobase (RPKM) of *PLAUR* mRNA in proliferating, quiescent (induced by serum starvation) or senescent (triggered by overexpression of $HRAS^{G12V}$) human IMR-90 fibroblasts. Results of one independent experiment with $n = 3$ replicates for proliferating, quiescent and senescent conditions. Data are mean ± s.e.m.; two-tailed unpaired Student's *t*-test.

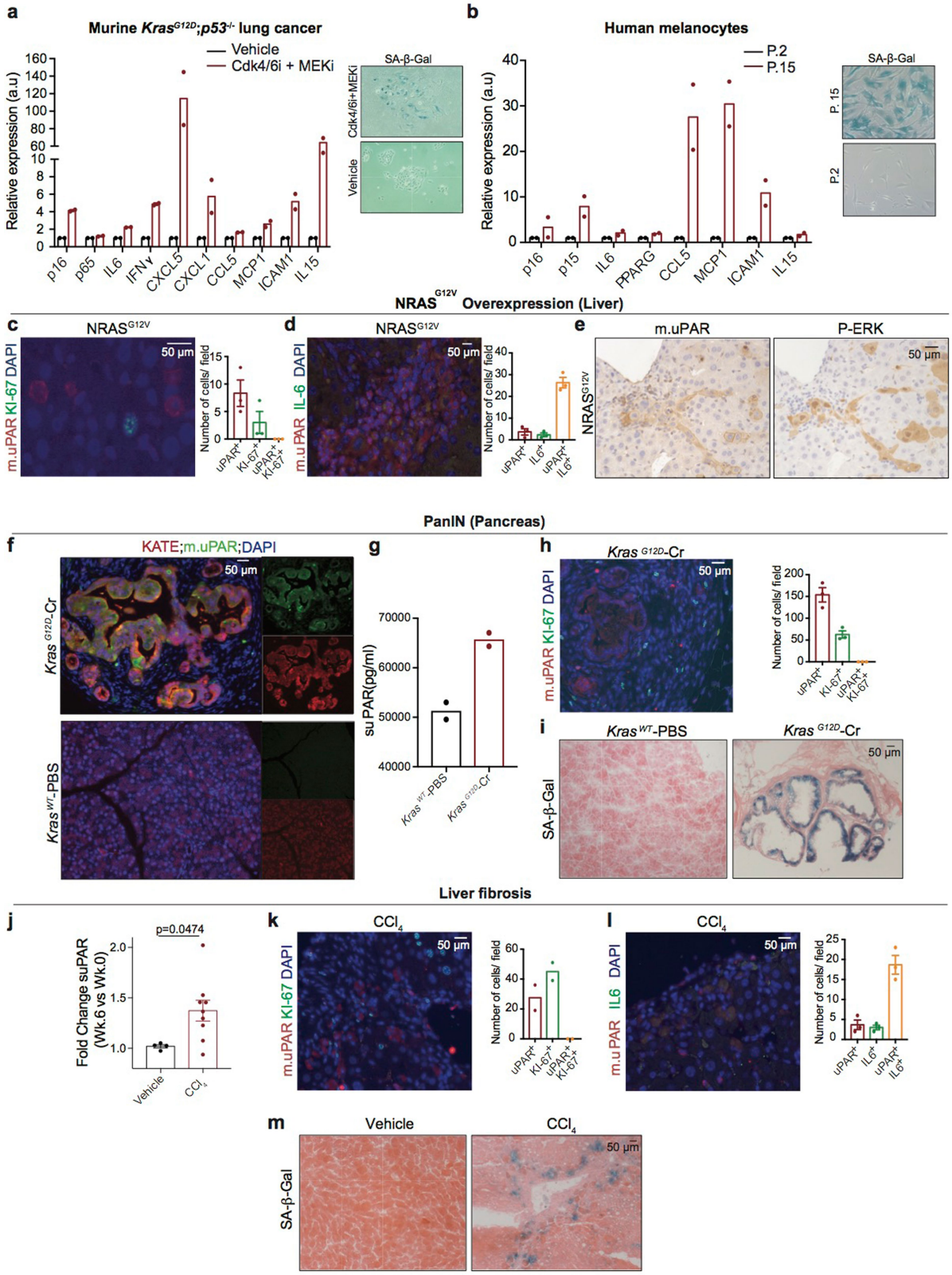

Extended Data Fig. 2 | See next page for caption.

Extended Data Fig. 2 | uPAR is a cell-surface and secreted biomarker of senescence. a, **b**, qPCR of SASP-associated gene expression in senescent versus proliferating mouse KP tumour cells (**a**) or human primary melanocytes (**b**) and representative SA-β-gal staining; a.u. arbitrary units. **c**, **d**, Co-immunofluorescence staining and quantifications of uPAR (red) and Ki-67 (green) (**c**) or uPAR (red) and IL-6 (green) (**d**). **e**, Immunohistochemical staining of uPAR or phosphorylated ERK (P-ERK) in serial sections of mouse livers six days after transfection by HTVI with a plasmid encoding $Nras^{G12V}$. Representative results of two independent experiments ($n = 3$ mice per group). **f**–**i**, Mice expressing endogenous $Kras^{G12D}$ in pancreatic epithelial cells were treated with caerulein (Cr) and euthanized 21 weeks afterwards when they had developed pancreatic intraepithelial neoplasias. Age-matched C;RIK mice (expressing wild-type *Kras*) injected with PBS were used as controls. **f**, Co-immunofluorescence staining of KATE (red) and uPAR (green). Representative results of two independent experiments ($n = 3$ mice per group). **g**, Levels of suPAR in the mice in **f**. Representative results of two independent experiments ($n = 2$ mice per group). **h**, Co-immunofluorescence staining and quantification of uPAR (red) and Ki-67 (green). Representative results of two independent experiments ($n = 3$ mice per group). **i**, Representative SA-β-gal staining. Representative results of one independent experiment ($n = 3$ mice per group). **j**–**m**, Mice were treated with either vehicle or CCl_4 twice weekly for six weeks to induce liver fibrosis. **j**, Fold change in serum levels of suPAR. Representative results of two independent experiments (vehicle, $n = 4$; CCl_4, $n = 9$ mice per group). Two-tailed unpaired Student's *t*-test. **k**, Co-immunofluorescence staining and quantification of uPAR (red) and Ki-67 (green). Representative results of two independent experiments ($n = 2$ mice per group). **l**, Co-immunofluorescence staining and quantification of uPAR (red) and IL-6 (green). Representative results of two independent experiments ($n = 3$ mice per group). **m**, Representative SA-β-gal staining. Representative results of two independent experiments ($n = 3$ mice per group). Data are mean ± s.e.m. (**c**, **d**, **h**, **j**, **l**).

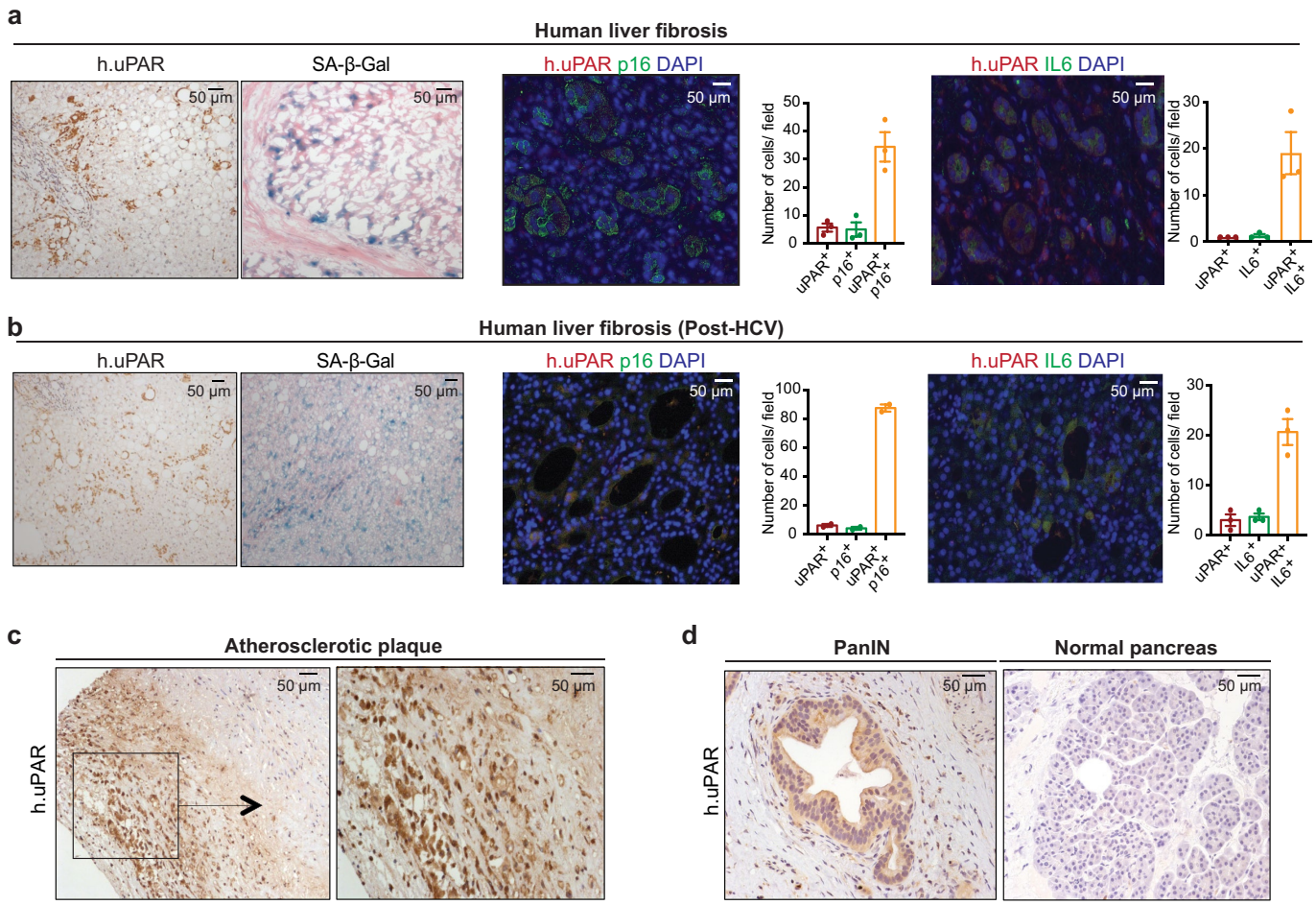

Extended Data Fig. 3 | uPAR is a marker of senescence in senescence-associated human pathologies. a, Left, immunohistochemical expression of human uPAR (h.uPAR) and SA-β-gal in human samples of hepatitis-induced liver fibrosis ($n = 7$ patients). Right, co-immunofluorescence staining and quantification of uPAR (red) and p16 (green) or uPAR (red) and IL-6 (green) in human samples of hepatitis-induced liver fibrosis ($n = 3$). **b**, Left, immunohistochemical expression of uPAR and SA-β-gal in human samples from patients with eradicated hepatitis C virus (HCV) and residual liver fibrosis ($n = 7$ patients). Right, co-immunofluorescence staining and quantification of uPAR (red) and p16 (green) or uPAR (red) and IL-6 (green) in human samples of HCV-induced liver fibrosis ($n = 3$). Data are mean ± s.e.m. (**a**, **b**). **c**, Immunohistochemical staining of uPAR in human carotid endarterectomy samples ($n = 5$ patients). **d**, Immunohistochemical staining of uPAR in human pancreas bearing pancreatic intraepithelial neoplasia (PanIN) compared to normal pancreas controls ($n = 3$ patients).

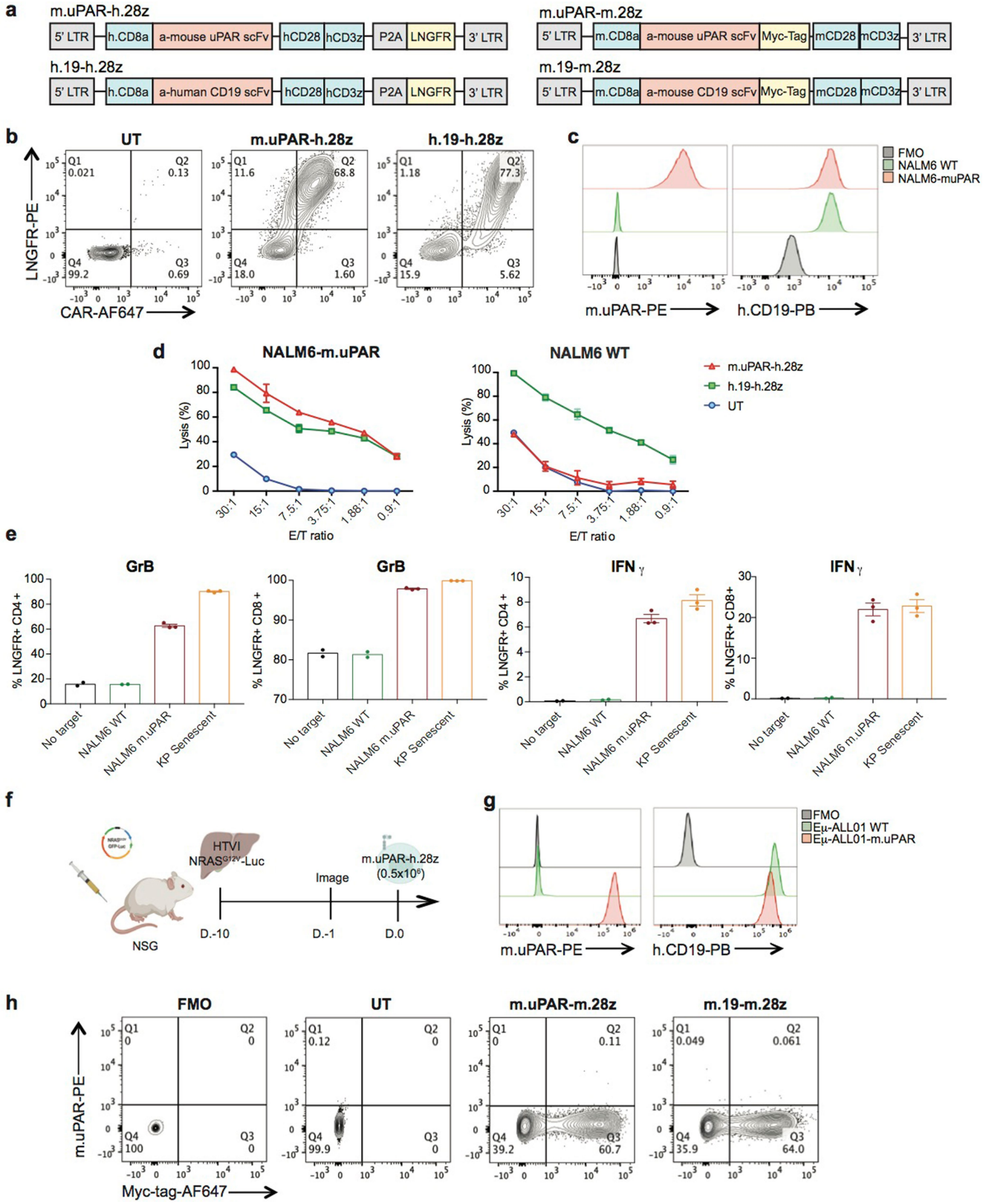

Extended Data Fig. 4 | See next page for caption.

Extended Data Fig. 4 | m.uPAR-h.28z CAR T cells selectively target uPAR-positive cells. a, Construct maps encoding human m.uPAR-h.28z and h.19-h.28z CARs or mouse m.uPAR-m.28z and m.19-m.28z CARs. **b**, Flow cytometry analysis showing the expression levels of CAR and LNGFR in m.uPAR-h.28z and h.19-h.28z CAR T cells compared to untransduced T cells. Representative results of $n = 4$ independent experiments. **c**, Flow cytometry analysis of mouse uPAR and human CD19 expression on wild-type NALM6 cells and NALM6-m.uPAR cells. Representative results of $n = 3$ independent experiments. **d**, Cytotoxic activity of m.uPAR-h.28z, h.19-h.28z and untransduced T cells as determined by 4-h calcein assay with firefly luciferase (FFL)-expressing NALM6 wild-type or NALM6-m.uPAR cells as targets. Representative results of $n = 3$ independent experiments performed in triplicate. Data are mean ± s.e.m. **e**, Granzyme B (GrB) and IFNγ expression of $CD4^+$ and $CD8^+$ m.uPAR-h.28z CAR T cells 18 h after co-culture with wild-type NALM6, NALM6-m.uPAR or senescent KP cells as determined by intracellular cytokine staining. Results of $n = 1$ independent experiment (no target and NALM6 WT, $n = 2$; NALM6-m.uPAR and KP senescent, $n = 3$ replicates). Data are mean ± s.e.m. **f**, Experimental layout for Fig. 2c–i. Mice were injected with a plasmid encoding $Nras^{G12V}$-GFP-luciferase and treated with 0.5×10^6 m.uPAR-h.28z CAR T cells or untransduced T cells 10 days after injection. Mice were euthanized 15 days after CAR administration and livers were used for further analysis. Images were created with BioRender.com. **g**, Flow cytometry analysis of mouse uPAR and human CD19 expression on wild-type Eμ-ALL01 cells and Eμ-ALL01-m.uPAR cells. Representative results of $n = 3$ independent experiments. **h**, Flow cytometry staining of Myc-tag and mouse uPAR on m.uPAR-m.28z CAR T cells, m.19-m.28z CAR T cells and untransduced T cells as compared to FMO control. Representative results of $n = 2$ independent experiments.

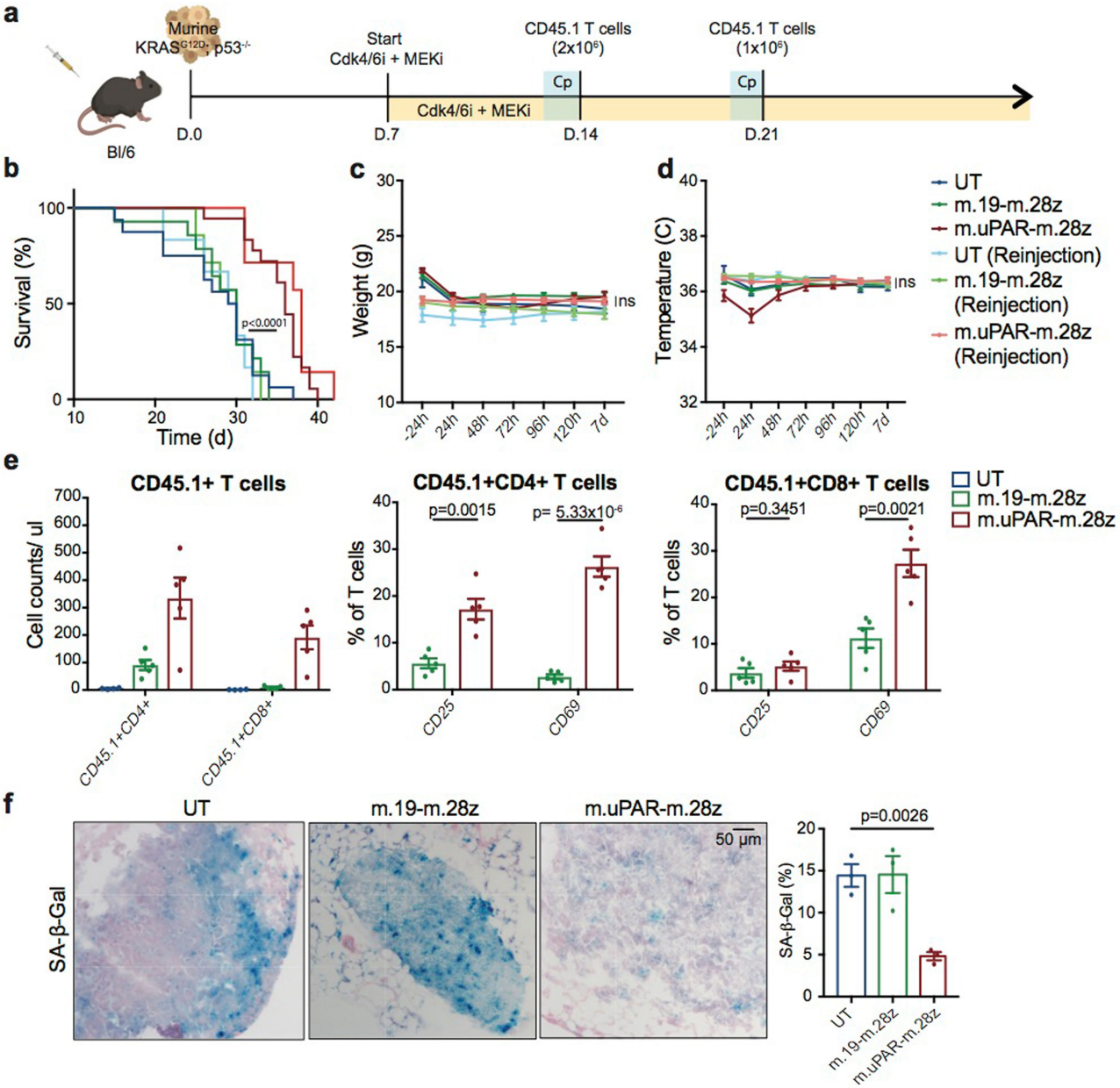

Extended Data Fig. 5 | Senolytic CAR T cells target senescent cells in a *Kras^{G12D}*-driven model of lung cancer. a, Experimental layout. C57BL/6N mice were intravenously injected with 10,000 *Kras^{G12D};p53$^{-/-}$* cells. Treatment with combined MEK inhibitor (1 mg per kg body weight) and CDK4/6 inhibitors (100 mg per kg body weight) was started seven days later, followed by adoptive transfer of 2×10^6 CD45.1$^+$ T cells (m.uPAR-m.28z CAR T cells, m.19-m.28z CAR T cells or untransduced T cells) one week later. A subset of mice received a second infusion of 1×10^6 m.uPAR-m.28z CAR T cells, m.19-m.28z CAR T cells or untransduced T cells seven days after the first injection of T cells. The images of the mouse, tumour cells and CAR T cells were created with BioRender.com. Cp, cyclophosphamide. **b**, Kaplan–Meier curve showing survival of mice (one-sided log-rank (Mantel–Cox) test). Results of two independent experiments (UT, $n = 16$; m.19-m.28z, $n = 14$; m.uPAR-m.28z, $n = 18$; UT reinjection, $n = 6$; m.19-m.28z reinjection, $n = 7$; m.uPAR-m.28z reinjection, $n = 7$ mice). **c**, **d**, Weight (**c**) and temperature (**d**) measured 24 h before and at different time points after CAR T cell infusion. *P* values (ns, not significant) refer to the comparison between untransduced and m.uPAR-m.28z injected mice at 48 h (weight, $P = 0.9329$; temperature, $P = 0.1534$). Results of one independent experiment (UT, $n = 5$; m.19-m.28z, $n = 5$; m.uPAR-m.28z, $n = 8$; UT reinjection, $n = 5$; m.19-m.28z reinjection, $n = 7$; m.uPAR-m.28z reinjection, $n = 7$ mice). **e**, Cell counts of CD45.1$^+$ T cells and expression of the activation markers CD25 and CD69 (UT, $n = 4$; m.19-m.28z, $n = 5$; m.uPAR-m.28z, $n = 5$ mice) on CD45.1$^+$ T cells in the lungs of mice seven days after administration of m.uPAR-m.28z CAR T cells, m.19-m.28z CAR T cells or untransduced T cells. **f**, Representative SA-β-gal staining and quantification in the lungs of mice seven days after treatment with m.uPAR-m.28z CAR T cells compared to mice that were treated with m.19-m.28z CAR T cells or untransduced T cells ($n = 3$ mice per group). Data are mean ± s.e.m.; two-tailed unpaired Student's *t*-test. (**c**–**f**).

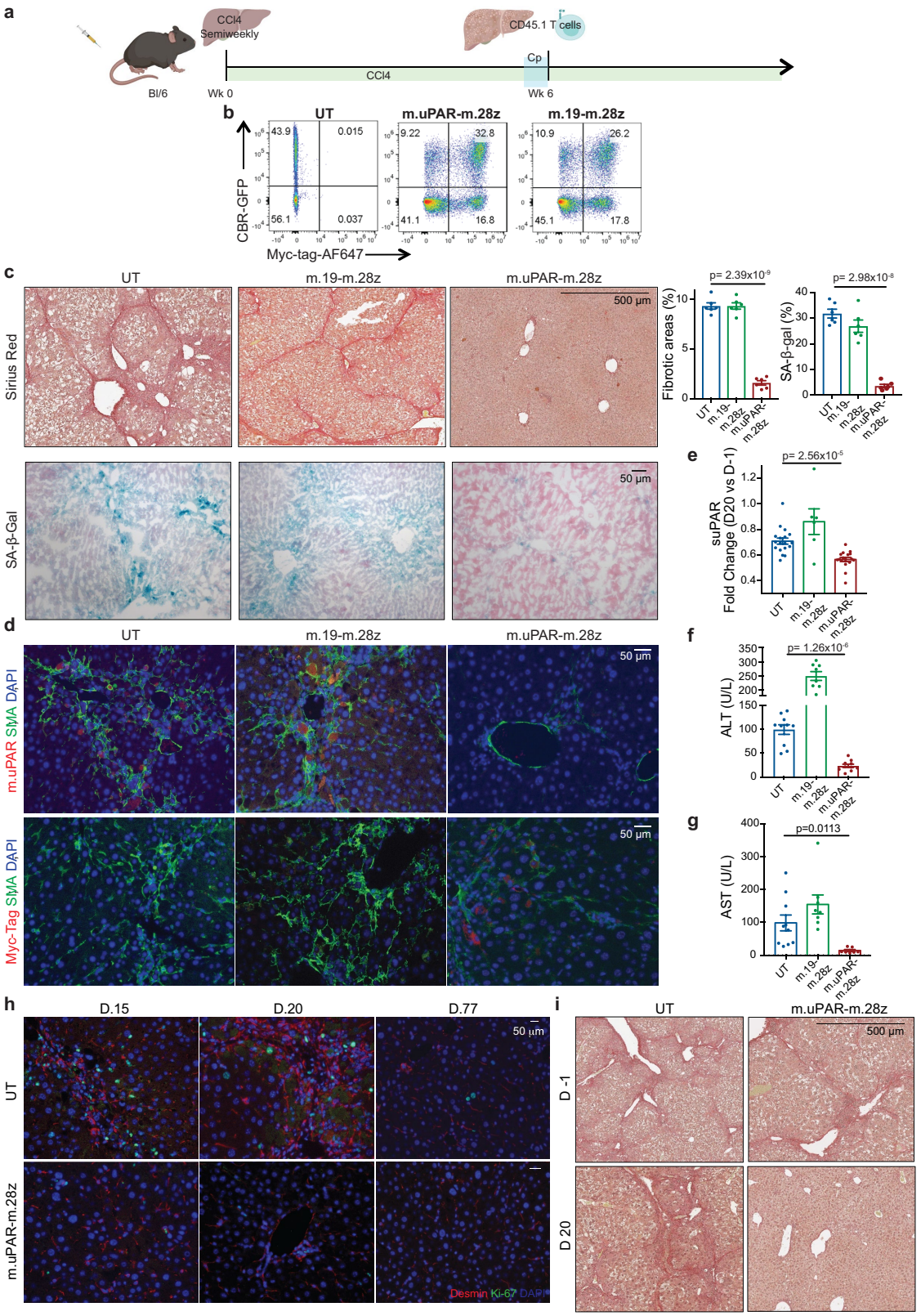

Extended Data Fig. 6 | See next page for caption.

Extended Data Fig. 6 | Senolytic CAR T cells show therapeutic activity in CCl_4-induced liver fibrosis. a, Layout for experiments performed using the CCl_4-induced liver fibrosis model: C57BL/6N mice received intraperitoneal infusions of CCl_4 twice weekly for six weeks and were intravenously infused with $0.5–1 \times 10^6$ (Fig. 3) or $2–3 \times 10^6$ (**c**–**i**) mouse m.uPAR-m.28z CAR T cells, m.19-m.28z CAR T cells or untransduced T cells 16–24 h after administration of cyclophosphamide (200 mg kg^{-1}). Mice were euthanized 20 days after CAR T cell infusion to assess liver fibrosis. Images were created with BioRender.com. **b**, Expression of GFP-tagged click beetle red (CBR) luciferase and Myc-tag in m.uPAR-m.28z and m.19-m.28z CAR T cells that were used for T cell imaging experiments (Fig. 3g, h) compared to control T cells. Representative results of $n = 2$ independent experiments. **c**, Sirius red and SA-β-gal staining and quantifications in livers from treated mice ($n = 6$ mice per group). **d**, Co-immunofluorescence of uPAR (red) and SMA (green) or Myc-tag (red) and SMA (green) in the livers of treated mice. **e**, Fold change difference in serum levels of suPAR 20 days after compared to 1 day before (day −1) injection of CAR T cells (UT, $n = 18$; m.19-m.28z, $n = 6$; m.uPAR-m.28z, $n = 17$ mice). **f**, **g**, Levels of serum ALT (**f**) and AST (**g**) 20 days after CAR treatment (UT, $n = 10$; m.19-m.28z, $n = 8$; m.uPAR-m.28z, $n = 10$ mice). **h**, Co-immunofluorescence staining of desmin (red) and Ki-67 (green) in the livers of mice 15, 20 and 77 days after treatment with CAR T cells. CCl_4 treatment was stopped 20 days after T cell infusion ($n = 3$ mice per group). **i**, Mice were treated with CCl_4 for 10 weeks. Sirius red staining in the livers of mice before (day −1) and 20 days after T cell administration (UT, $n = 4$; m.uPAR-m.28z, $n = 2$ mice). Representative results of $n = 2$ independent experiments (**c**–**i**). Data are mean ± s.e.m.; two-tailed unpaired Student's *t*-test (**c**, **e**–**g**).

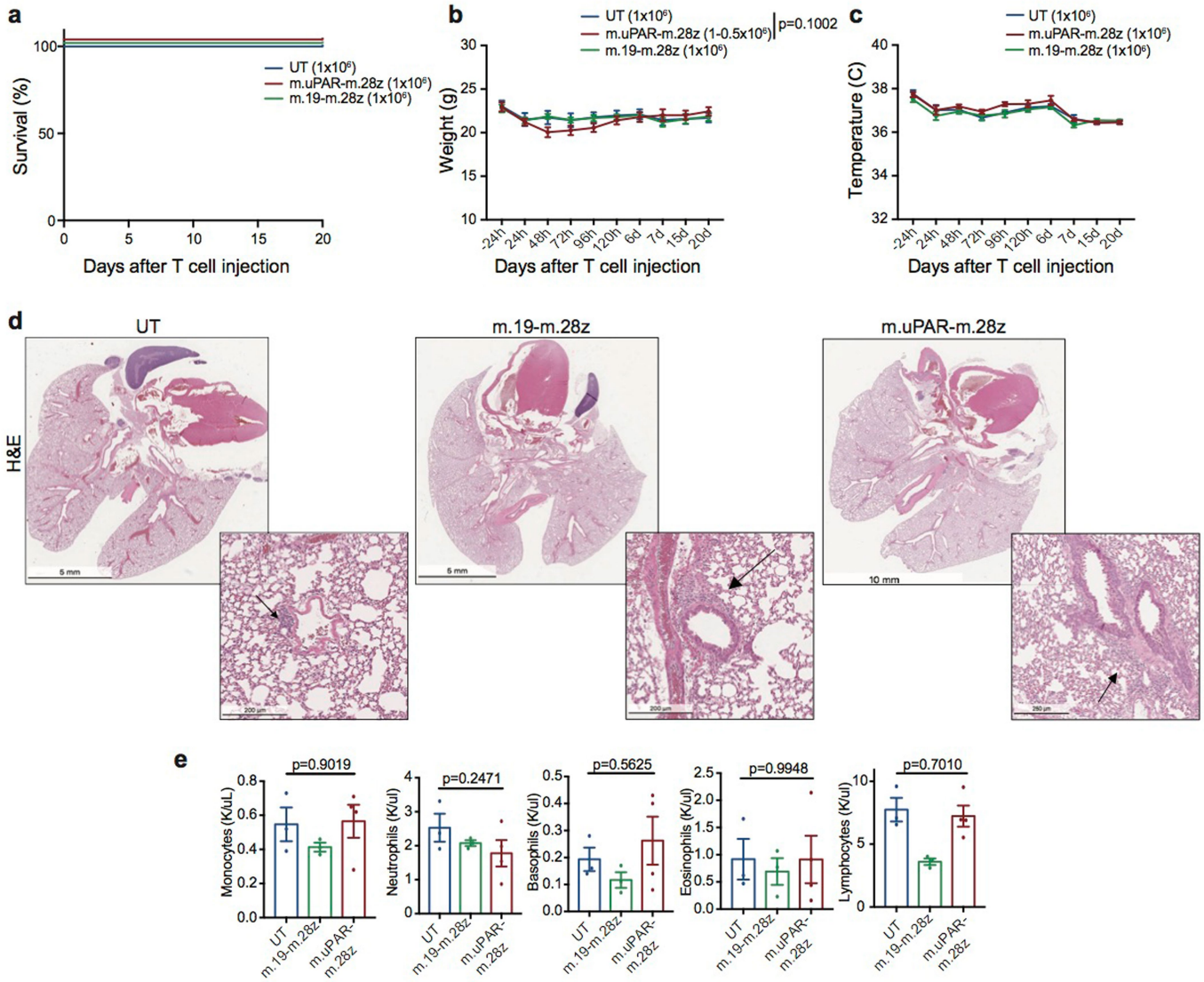

Extended Data Fig. 7 | Safety profile of m.uPAR-m.28z CAR T cells at therapeutic doses of T cells. a–**e**, C57BL/6N mice received intraperitoneal infusions of CCl_4 twice weekly for six weeks and were intravenously injected with 0.5–1 × 10^6 m.uPAR-m.28z CAR T cells, 1 × 10^6 m.19-m.28z CAR T cells or untransduced T cells 16 h after administration of cyclophosphamide (200 mg kg^{-1}). Mice were euthanized 20 days after T cell administration to assess potential toxicities and lung histopathology. **a**, Kaplan–Meier curve showing survival of mice after treatment with m.uPAR-m.28z CAR T cells (n = 16 mice), m.19-m.28z CAR T cells (n = 6 mice) or untransduced T cells (n = 6 mice). **b**, **c**, Weight (**b**) and temperature (**c**) of mice measured before and at different time points after CAR T cell infusion (UT and m.19-m.28z, n = 6; m.uPAR-m.28z, n = 7 mice). The P value in **b** refers to differences in weight at 48 h. **d**, **e**, Representative H&E staining of lungs (**d**) and complete blood counts (**e**) of treated mice 20 days after T cell infusion (UT and m.19-m.28z, n = 3 or 4; m.uPAR-m.28z, n = 4 mice). An increased accumulation of macrophages was observed in the immunodeficient setting. Representative results of n = 1 independent experiment (**a**–**e**). Data are mean ± s.e.m. (**b**, **c**, **e**); two-tailed unpaired Student's t-test (**b**, **e**).

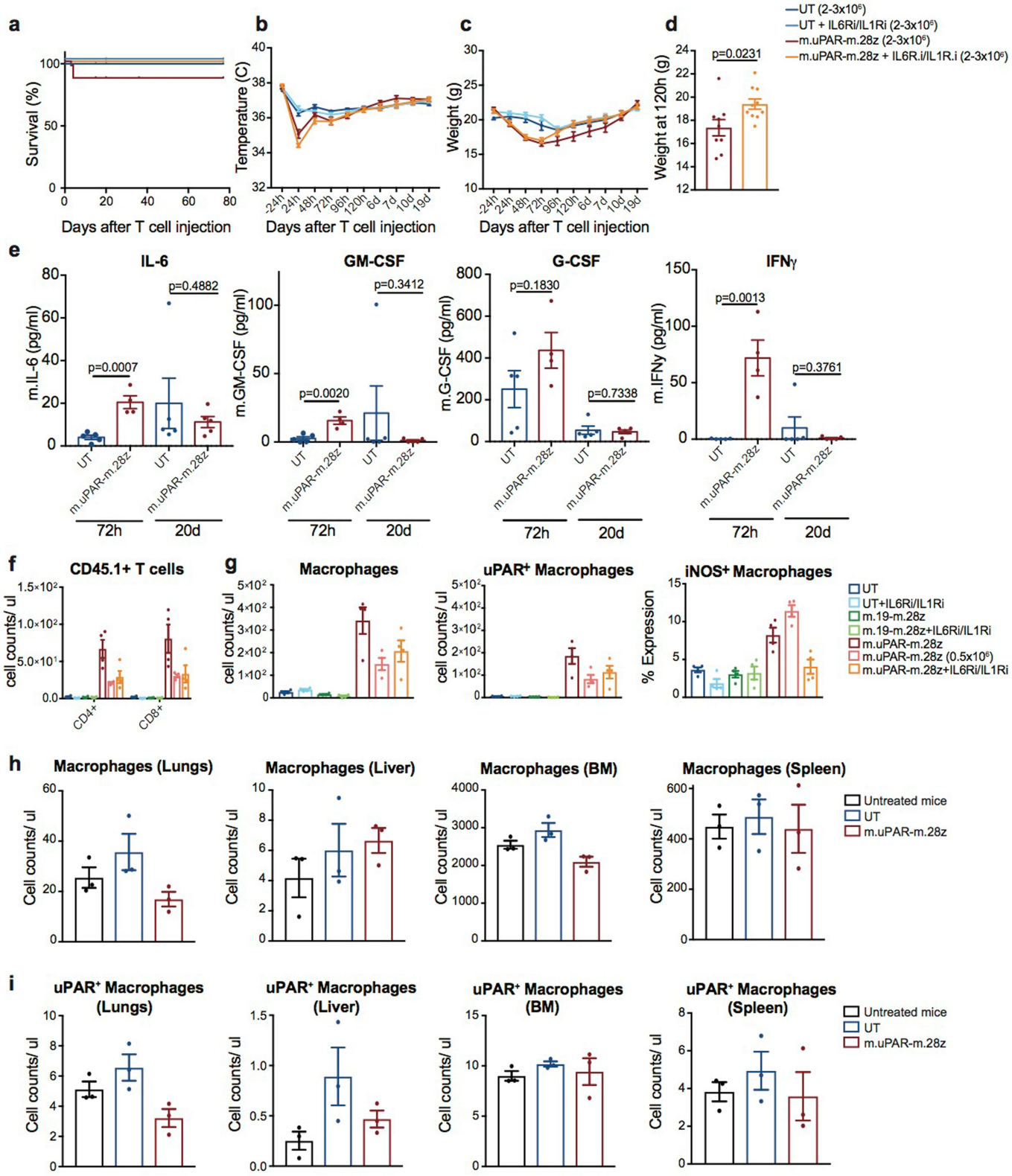

Extended Data Fig. 8 | See next page for caption.

Extended Data Fig. 8 | Safety profile of m.uPAR-m.28z CAR T cells at supratherapeutic doses of T cells. C57BL/6N mice received intraperitoneal infusions of CCl_4 twice weekly for six weeks followed by intravenous infusion of $2–3 \times 10^6$ m.uPAR-m.28z CAR T cells or untransduced T cells 16–24 h after administration of cyclophosphamide (200 mg kg^{-1}). A subset of mice (as specified in the figure) received additional treatment with IL-6R-blocking antibodies (IL6Ri) and the IL-1R antagonist anakinra (IL1Ri), starting 24 h before T cell infusion and continuing daily until 6 days after T cell infusion. Mice were euthanized 12 weeks after CAR infusion to assess potential toxicities. **a**, Kaplan–Meier curve showing survival of mice after injection of CAR T cells (UT, $n = 19$; UT + IL6Ri/IL1Ri, $n = 7$; m.uPAR-m.28z, $n = 30$; m.uPAR-m.28z + IL6Ri/IL1Ri, $n = 19$ mice). **b**, **c**, Temperature (**b**) and weight (**c**) of treated mice (UT, $n = 7$; UT + IL6Ri/IL1Ri, $n = 8$; m.uPAR-m.28z, $n = 11$; m.uPAR-m.28z + IL6Ri/IL1Ri, $n = 10$ mice). **d**, Weight of mice 120 h after infusion with either m.uPAR-m.28z or m.uPAR-m.28z CAR T cells and additional treatment with IL6Ri and IL1Ri (m.uPAR-m.28z, $n = 11$; m.uPAR-m.28z + IL6Ri/IL1Ri, $n = 10$ mice). **e**, Serum levels of IL-6, GM-CSF, G-CSF and IFNγ in mice that were treated with either m.uPAR-m.28z or untransduced T cells 72 h or 20 days after T cell infusion (UT, $n = 5$; m.uPAR-m.28z, $n = 4$ mice at 72 h; $n = 5$ mice at 20 days). **f**, **g**, Number of adoptively transferred $CD45.1^+$ T cells (**f**) and number of macrophages, $uPAR^+$ and $iNOS^+$ macrophages (**g**) in the lungs of mice that were treated with m.uPAR-m.28z CAR T cells, m.19-m.28z CAR T cells or untransduced T cells alone or in combination with treatment with IL6Ri and ILR1Ri three days after T cell infusion ($n = 4$ mice per group). **h**, **i**, Number of macrophages (**h**) and $uPAR^+$ macrophages (**i**) in the lungs, liver, bone marrow (BM) and spleen of untreated mice or mice treated with either m.uPAR-m.28z CAR T cells or untransduced T cells 12 weeks after T cell infusion ($n = 3$ mice per group). Representative results of $n = 3$ independent experiments (**a**–**d**) or $n = 1$ independent experiment (**e**–**i**). All data are mean ± s.e.m.; two-tailed unpaired Student's *t*-test (**d**, **e**).

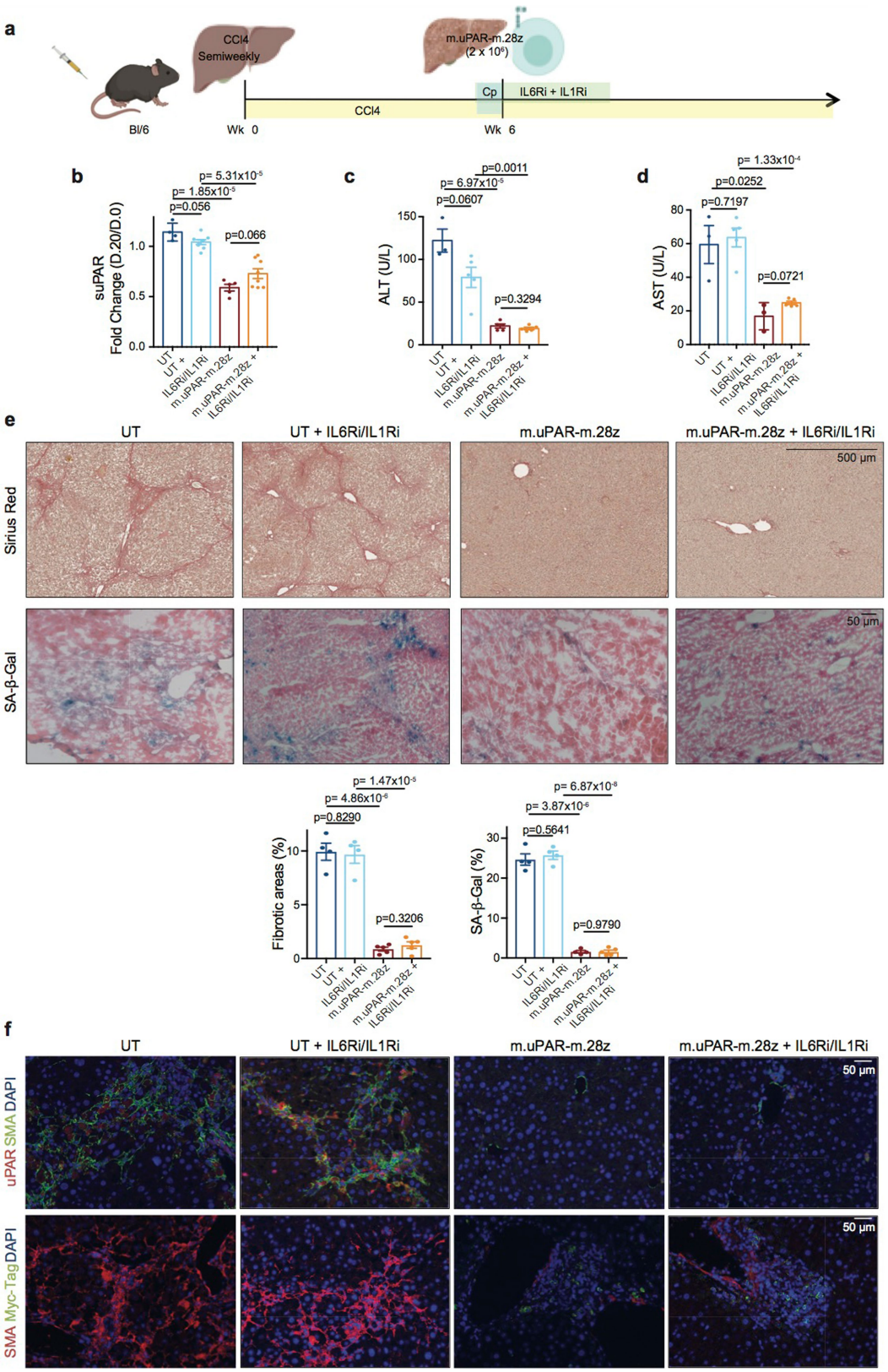

Extended Data Fig. 9 | See next page for caption.

Extended Data Fig. 9 | Therapeutic intervention with IL-6R and IL-1R inhibitors does not decrease the therapeutic efficacy of senolytic CAR T cells in CCl_4-induced liver fibrosis. a, Experimental layout. C57BL/6N mice received intraperitoneal infusions of CCl_4 twice weekly for six weeks and were intravenously infused with $2–3 \times 10^6$ m.uPAR-m.28z CAR T cells or untransduced T cells 24 h after administration of cyclophosphamide ($200\ mg\ kg^{-1}$). IL-6R-blocking antibodies (IL6Ri) and anakinra (ILRi) were first administered 24 h before T cell infusion followed by daily (IL6Ri) or twice daily (IL1Ri) injections for the first six days until treatment was stopped. Mice were euthanized 20 days after T cell infusion to assess liver fibrosis. Images were created with BioRender.com. **b**, Fold change difference in serum levels of suPAR 20 days after compared to 1 day before (day −1) CAR T cell treatment (UT, $n = 4$; UT + IL6Ri/IL1Ri, $n = 8$; m.uPAR, $n = 5$; m.uPAR + IL6Ri/IL1Ri, $n = 8$ mice). **c**, **d**, Levels of serum ALT (**c**) and AST (**d**) in treated mice 20 days after T cell infusion (UT, $n = 3$; UT + IL6Ri/IL1Ri, $n = 5$; m.uPAR-m.28z, $n = 5$ (ALT) and $n = 3$ (AST); m.uPAR-m.28z + IL6Ri/IL1Ri, $n = 5$ mice). **e**, Representative levels of fibrosis evaluated by Sirius red staining and SA-β-gal staining in livers from treated mice and quantification of liver fibrosis and SA-β-gal$^+$ cells in the respective livers 20 days after treatment (UT, $n = 4$; UT + IL6Ri/IL1Ri, $n = 4$; m.uPAR-m.28z, $n = 4$; m.uPAR-m.28z + IL6Ri/IL1Ri, $n = 5$ mice). **f**, Co-immunofluorescence staining of uPAR (red) and SMA (green) or Myc-tag (red) and SMA (green) in the livers of treated mice. Representative results of $n = 1$ independent experiment (**b**–**f**). Data are mean ± s.e.m.; two-tailed unpaired Student's *t*-test (**b**–**e**).

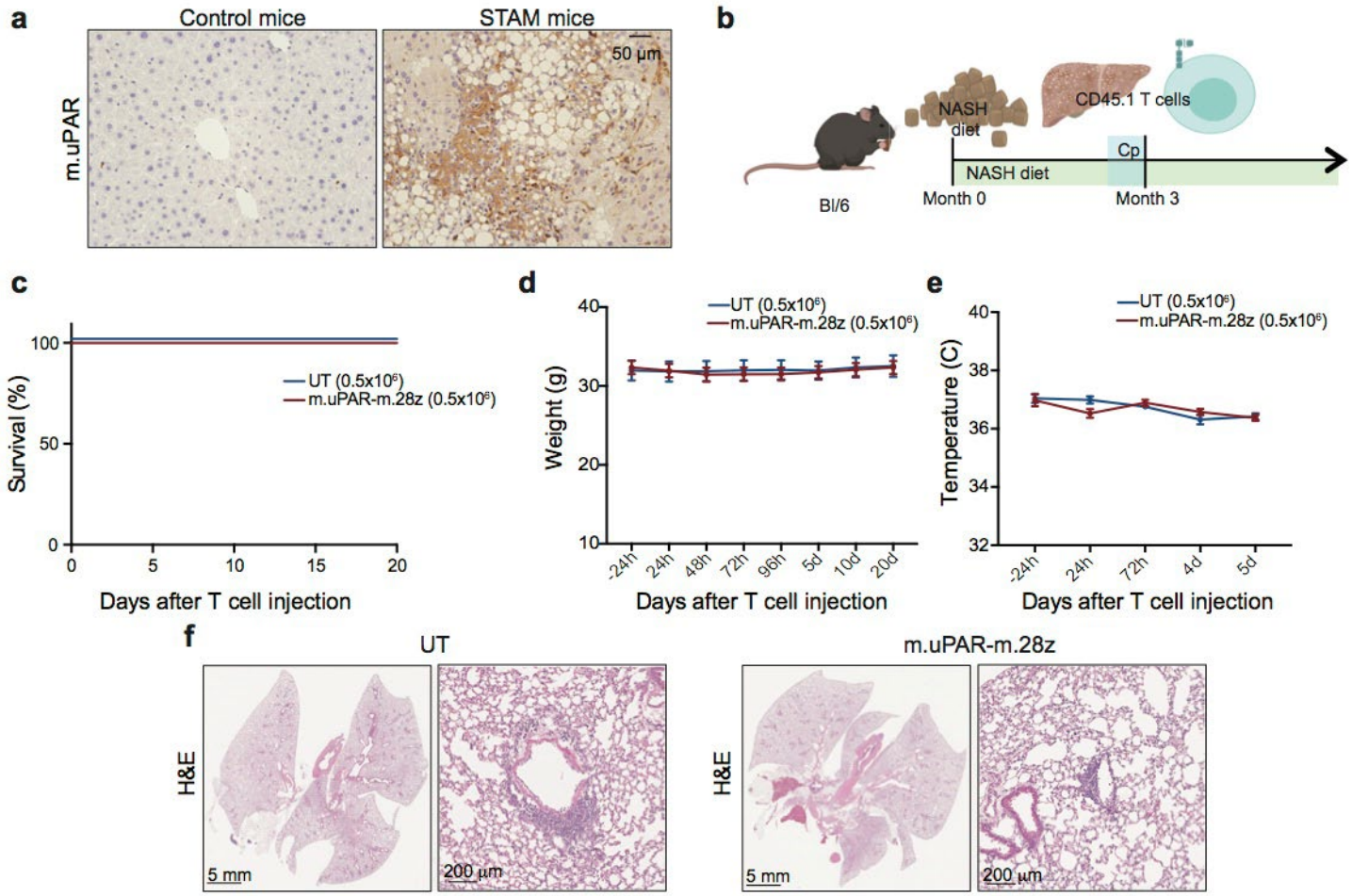

Extended Data Fig. 10 | Safety profile of senolytic CAR T cells at therapeutic doses in a mouse model of NASH-induced liver fibrosis. **a**, Immunohistochemical expression of uPAR in samples from the 'STAM' model[52,58] ($n = 3$ mice). **b**, Experimental layout for experiments performed using the model of diet-induced NASH (Fig. 4, this figure). C57BL/6N mice were treated with a chow or a NASH-inducing diet[50] for three months, followed by intravenous infusion with 0.5×10^6 m.uPAR-m.28z CAR T cells or untransduced T cells 16 h after administration of cyclophosphamide (200 mg kg^{-1}). Mice were euthanized 20 days after CAR infusion to assess liver fibrosis. Images were created with BioRender.com. **c**, Kaplan–Meier curve showing survival of mice after treatment with either m.uPAR-m.28z CAR T cells or untransduced T cells (m.uPAR-m.28z, $n = 16$; UT, $n = 10$ mice). **d**, **e**, Weight (**d**) and temperature (**e**) of mice 24 h before and at different time points after T cell infusion (m.uPAR-m.28z, $n = 11$; UT, $n = 9$ mice). Data are mean ± s.e.m. **f**, Representative H&E staining of the lungs of treated mice (m.uPAR-m.28z, $n = 6$; UT, $n = 4$ mice). Representative results of $n = 2$ independent experiments (**c**–**f**).

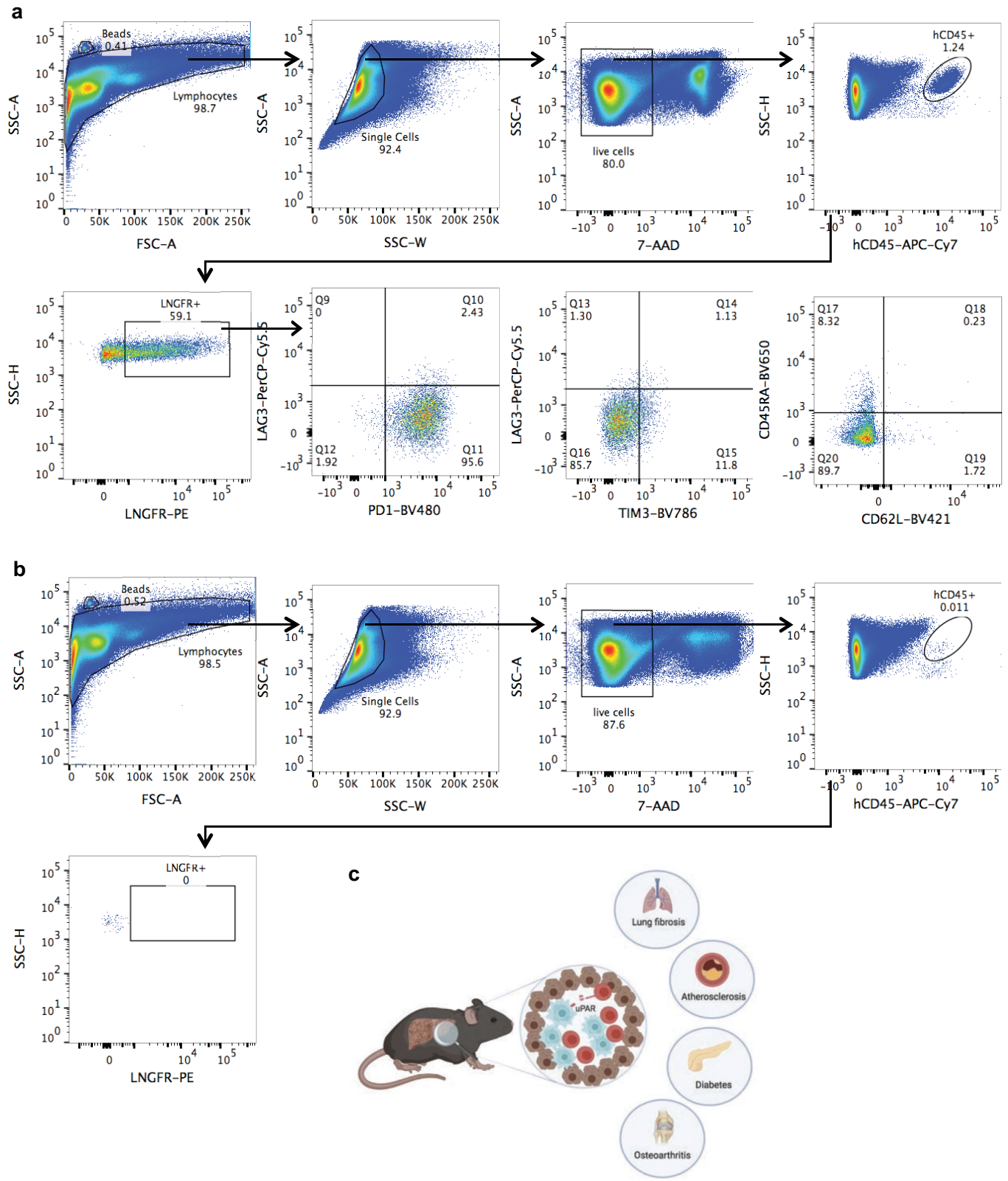

Extended Data Fig. 11 | Gating strategies, summary and potential applications of senolytic CAR T cells. a, **b**, Representative flow cytometry staining of m.uPAR-h.28z CAR T cells (**a**) or untransduced T cells (**b**) obtained from the livers of mice that had undergone HTVI (as depicted in Fig. 2). Representative results of one independent experiment ($n = 4$ mice per group). **c**, Summary of the key points of our findings. uPAR-28z CAR T cells (red) infiltrate fibrotic livers that contain senescent cells (blue) and efficiently eliminate them, leading to fibrosis resolution and improved liver function. The therapeutic action of senolytic uPAR-28z CAR T cells might be extended to other senescence-associated diseases such as atherosclerosis, diabetes or osteoarthritis. Images were created with BioRender.com.

nature research

Corresponding author(s): Scott W Lowe

Last updated by author(s): April 22, 2020

Reporting Summary

Nature Research wishes to improve the reproducibility of the work that we publish. This form provides structure for consistency and transparency in reporting. For further information on Nature Research policies, see Authors & Referees and the Editorial Policy Checklist.

Statistics

For all statistical analyses, confirm that the following items are present in the figure legend, table legend, main text, or Methods section.

n/a	Confirmed	
☐	☒	The exact sample size (*n*) for each experimental group/condition, given as a discrete number and unit of measurement
☐	☒	A statement on whether measurements were taken from distinct samples or whether the same sample was measured repeatedly
☐	☒	The statistical test(s) used AND whether they are one- or two-sided *Only common tests should be described solely by name; describe more complex techniques in the Methods section.*
☒	☐	A description of all covariates tested
☐	☒	A description of any assumptions or corrections, such as tests of normality and adjustment for multiple comparisons
☐	☒	A full description of the statistical parameters including central tendency (e.g. means) or other basic estimates (e.g. regression coefficient) AND variation (e.g. standard deviation) or associated estimates of uncertainty (e.g. confidence intervals)
☐	☒	For null hypothesis testing, the test statistic (e.g. *F*, *t*, *r*) with confidence intervals, effect sizes, degrees of freedom and *P* value noted *Give P values as exact values whenever suitable.*
☒	☐	For Bayesian analysis, information on the choice of priors and Markov chain Monte Carlo settings
☒	☐	For hierarchical and complex designs, identification of the appropriate level for tests and full reporting of outcomes
☒	☐	Estimates of effect sizes (e.g. Cohen's *d*, Pearson's *r*), indicating how they were calculated

Our web collection on statistics for biologists contains articles on many of the points above.

Software and code

Policy information about availability of computer code

Data collection	BD LSR-II and BD LSR-Fortessa cytometer, Cytek Aurora (CYTEK), Xenogen IVIS Imaging System living image V4.4, Microsoft Excel for Mac 2011.
Data analysis	FlowJo 10.1 , GraphPad Prism V6 and V7, Living Image 4.4, Image J, version 2.0.0-rc-43/1.51h. RNAseq analysis was performed with the following software: HTSeq v0.5.3, picard tools v1.124, R v3.2.0, STAR v2.5.0a, samtools v0.1.19, Microsoft Excel for Mac 2011.

For manuscripts utilizing custom algorithms or software that are central to the research but not yet described in published literature, software must be made available to editors/reviewers. We strongly encourage code deposition in a community repository (e.g. GitHub). See the Nature Research guidelines for submitting code & software for further information.

Data

Policy information about availability of data

All manuscripts must include a data availability statement. This statement should provide the following information, where applicable:

- Accession codes, unique identifiers, or web links for publicly available datasets
- A list of figures that have associated raw data
- A description of any restrictions on data availability

The RNA-seq data has been deposited in the Gene Expression Omnibus (GEO) under the accession number GSE145642.
The datasets generated during the current study are available from the corresponding author upon reasonable request.

Field-specific reporting

Please select the one below that is the best fit for your research. If you are not sure, read the appropriate sections before making your selection.

☒ Life sciences ☐ Behavioural & social sciences ☐ Ecological, evolutionary & environmental sciences

For a reference copy of the document with all sections, see nature.com/documents/nr-reporting-summary-flat.pdf

Life sciences study design

All studies must disclose on these points even when the disclosure is negative.

Sample size	No statistical methods were used to pre-determine sample size. Sample sizes were estimated based on preliminary experiments, with an effort to achieve a minimum of n=5 mice per treatment group which proved to be sufficient to reproducibly observe a statistically significant difference.
Data exclusions	No data were excluded throughout the studies.
Replication	All in vitro and in vivo experiments were repeated in replicates and/or from different subjects in independent experiments. All attempts at replication were successful. Efficacy of CAR T cell treatment may vary between donors.
Randomization	Senescence burden for HTVI was determined by bioluminescent imaging one day prior to CAR T cell transfer and by suPAR measurement in the liver fibrosis model. Since senescent burdens were very even, mice were randomly assigned into treatment groups. Buffy coats were obtained from anonymous donors.
Blinding	Mouse conditions were observed by an operator who was blinded to the treatment groups in addition to the main investigator who was not blind to group allocation. Analysis of data was not performed in blinded fashion. Data analysis are based on objectively measurable data (fluorescence intensity, cell count, blood tests).

Reporting for specific materials, systems and methods

We require information from authors about some types of materials, experimental systems and methods used in many studies. Here, indicate whether each material, system or method listed is relevant to your study. If you are not sure if a list item applies to your research, read the appropriate section before selecting a response.

Materials & experimental systems

n/a	Involved in the study
☐	☒ Antibodies
☐	☒ Eukaryotic cell lines
☒	☐ Palaeontology
☐	☒ Animals and other organisms
☐	☒ Human research participants
☒	☐ Clinical data

Methods

n/a	Involved in the study
☒	☐ ChIP-seq
☐	☒ Flow cytometry
☒	☐ MRI-based neuroimaging

Antibodies

Antibodies used

The following fluorophore-conjugated antibodies were used ("h" prefix denotes anti-human, "m" prefix denotes anti-mouse): hCD45 APC-Cy7 (clone 2D1, BD, #557833, Lot: 9081815, 1:100), hCD4 BUV395 (clone SK3, BD, #563550, Lot: 6252529, 1:100), hCD4 BV480 (clone SK3, BD, #566104, Lot: 8092993, 1:50.), hCD62L BV421 (clone DREG-56, BD, #563862, Lot: 8194954, 1:100.), hCD45RA BV650 (clone HI100, BD, #563963, Lot: 9057952, 1:100.), hPD1 BV480 (clone EH12.1, BD, #566112, Lot: 8235507, 1:100.), hCD19 BUV737 (clone SJ25C1, BD, #564303, Lot: 8130572, 1:100.), hCD271 PE (clone C40-1457, BD, #557196, Lot: 7068641, 1:100.), hIL2 PE-Cy7 (clone MQ1-17H12, Invitrogen, #25-7029-42, Lot: 4336863, 1:50.), hTNFa BV650 (clone Mab11, BD, #563418, Lot: 7082880, 1:50.), hIFNg BUV395 (clone B27, BD, #563563, Lot: 6320836, 1:50.) hTIM3 BV785 (clone F38-2E2, Biolegend, #345032, Lot: B265346, 1:100.), hCD8 PE-Cy7 (clone SK1, eBioscience, #25-0087-42, Lot: 2066348, 1:100.), hCD8 APC-Cy7 (clone SK1, BD, #557834, Lot: 7110951, 1:50.), hCD223 PerCP-eFluor710 (clone 3DS223H, eBioscience, #46-2239-42, Lot: 4321735, 1:100.), hGrB APC (clone GB12, Invitrogen, #MHGB05, Lot: 1884625, 1:67.), hMyc-tag AF647 (clone 9B11, Cell Signaling Technology, #2233S, Lot: 23, 1:50.), hCD19 PB (clone SJ25-C1, Invitrogen, #MHCD1928, 1:100.), hCD87 APC (clone VIM5, eBioscience, #17-3879-42, Lot: 17-3879-42, 1:50.), hCD87 PerCp-eFluor710 (clone VIM5, eBioscience, #46-3879-42, Lot: 46-2239-42, 1:50.), muPAR PE (R&D Systems, FAB531P, Lot: ABLH0419081, 1:50.), muPAR AF700 (R&D Systems, FAB531N, Lot: 1552229, 1:50.), mCD45.1 APC-Cy7 (clone A20, Biolegend, #110716, Lot: B285685, 1:200.), m.CD45.1 BV785 (clone A20, Biolegend, #110743, Lot: B270183, 1:100.), mCD45.2 PE (clone 104, Biolegend, #109808, Lot: B271929, 1:100.), mCD45.2 AF700 (clone 104, Biolegend, #109822, Lot: B252126, 1:200.), mSiglec-F PerCP-Cy5.5 (clone E50-2440, BD, #565526, Lot: 8232650, 1:200.), mI-A/I-E BV605 (clone M5/114.15.2, Biolegend, #107639, Lot: B293222, 1:50.), mF4/80 BV421 (clone: T45-2342, BD, #565411, Lot: 8330526, 1:200.), mCD11b BUV395 (clone: M1/70, BD, #563553, Lot: 8339988, 1:200.), mCD11c BV650 (clone: N418, Biolegend, #117339, Lot: B253523, 1:200.), mLY6G BV510 (clone: 1A8, Biolegend, #127633, Lot: B266675, 1:200.), mLY6G

APC/Fire750 (clone: 1A8, Biolegend, #127652, Lot: B274284, 1:100.), miNOS PE-Cy7 (clone: CXNFT, eBioscience, #25-5920-82, Lot: 2127491, 1:200.), mCD19 PE (clone 1D3/CD19, Biolegend, #152408, Lot: B260181, 1:100.), mCD25 BV605 (clone: PC61, Biolegend, #102035, Lot: B291215, 1:50.), mCD69 PerCpCy5.5 (clone: H1.2F3, Biolegend, #104522, Lot: B244018, 1:100.), mCD3 AF488 (clone: 17A2, Biolegend, #100210, Lot: B284975, 1:100.), mCD4 BUV395 (clone: GK1.5, BD, #563790, Lot: 9101822, 1:50.), mCD4 FITC (clone: GK1.5, BD, #553729, Lot: 9204449, 1:50.), mCD8 PE-Cy7 (Clone: 53-6.7, Biolegend, #100722, Lot: B282418, 1:50.),Alexa Fluor 647 AffiniPure F(ab)2 Fragment Goat Anti-Rat IgG (Jackson ImmunoResearch, #112-6606-072), huPAR (R&D. AF807 Lot.BBS0318071. 1:50), muPAR (R&D. AF534 Lot.DCL0418021. 1:50), mNRAS (Santa Cruz. SC-31 Lot.A1020. 1:50), mSMA (abcam. Ab5694 Lot.GR283004-16. 1:50), mKATE (Evrogen. ab233 Lot.23301201267. 1:1000), hCD3 (abcam. ab5690 Lot.GR3220039-4. 1:100), myc-tag (Cell Signaling. 2276S Lot.24. 1:50), mKi-67 (abcam, ab16667 Lot.GR3305281-1. 1:200), mIL-6 (abcam. ab6672 Lot.GR3195128-19. 1:50), p16-INK4A (Proteintech. 10883-1-AP Lot.00057396. 1:50), mP-ERKT202/Y204 (Cell Signaling.4370 Lot.15. 1:800), desmin (ThermoFisher Scientific . RB-9014 Lot.9014p1806Q. 1:200), AF488 donkey anti-rabbbit (Invitrogen. A21206 Lot.1874771. 1:500), AF488 donkey anti-mouse (Invitrogen. A21202 Lot.1820538. 1:500), AF594 donkey anti-rabbit (Invitrogen. A21207 Lot.1602780. 1:500), AF594 donkey anti-mouse (Invitrogen A21203 Lot.1163390. 1:500), AF594 donkey anti-goat (Invitrogen. A11058 Lot.2045324. 1:500), AF594 goat anti-rat (Invitrogen A11007 Lot.1903506. 1:500).

Validation

All used antibodies were titrated. All the antibodies are validated for use in flow cytometry or immunohistochemistry or immunofluorescence. Data are available on the manufacturer's website. The following primary antibodies have been validated by the manufacturer in the mentioned species: hCD45 APC-Cy7 (clone 2D1, BD, #557833, Human), hCD4 BUV395 (clone SK3, BD, #563550, Human), hCD4 BV480 (clone SK3, BD, #566104, Human), hCD62L BV421 (clone DREG-56, BD, #563862, Human), hCD45RA BV650 (clone HI100, BD, #563963, Human), hPD1 BV480 (clone EH12.1, BD, #566112, Human), hCD19 BUV737 (clone SJ25C1, BD, #564303, Human), hCD271 PE (clone C40-1457, BD, #557196, Human), hIL2 PE-Cy7 (clone MQ1-17H12, Invitrogen, #25-7029-42, Human), hTNFa BV650 (clone Mab11, BD, #563418, Human), hIFNg BUV395 (clone B27, BD, #563563, Human), hTIM3 BV785 (clone F38-2E2, Biolegend, #345032, Human), hCD8 PE-Cy7 (clone SK1, eBioscience, #25-0087-42, Human), hCD8 APC-Cy7 (clone SK1, BD, #557834, Human), hCD223 PerCP-eFluor710 (clone 3DS223H, eBioscience, #46-2239-42, Human), hGrB APC (clone GB12, Invitrogen, #MHGB05, Human), hMyc-tag AF647 (clone 9B11, Cell Signaling Technology, #2233S, Transfected mammalian cells), hCD19 PB (clone SJ25-C1, Invitrogen, #MHCD1928, Human), hCD87 APC (clone VIM5, eBioscience, #17-3879-42, Human), hCD87 PerCp-eFluor710 (clone VIM5, eBioscience, #46-3879-42, Human), muPAR PE (R&D Systems, FAB531P, Mouse), muPAR AF700 (R&D Systems, FAB531N, Mouse), mCD45.1 APC-Cy7 (clone A20, Biolegend, #110716, Mouse), m.CD45.1 BV785 (clone A20, Biolegend, #110743, Mouse), mCD45.2 PE (clone 104, Biolegend, #109808, Mouse), mCD45.2 AF700 (clone 104, Biolegend, #109822, Mouse), mSiglec-F PerCP-Cy5.5 (clone E50-2440, BD, #565526, Mouse), mI-A/I-E BV605 (clone M5/114.15.2, Biolegend, #107639, Mouse), mF4/80 BV421 (clone: T45-2342, BD, #565411, Mouse), mCD11b BUV395 (clone: M1/70, BD, #563553, Mouse), mCD11c BV650 (clone: N418, Biolegend, #117339, Mouse), mLY6G BV510 (clone: 1A8, Biolegend, #127633, Mouse), mLY6G APC/Fire750 (clone: 1A8, Biolegend, #127652, Mouse), miNOS PE-Cy7 (clone: CXNFT, eBioscience, #25-5920-82, Mouse), mCD19 PE (clone 1D3/CD19, Biolegend, #152408, Mouse), mCD25 BV605 (clone: PC61, Biolegend, #102035, Mouse), mCD69 PerCpCy5.5 (clone: H1.2F3, Biolegend, #104522, Mouse), mCD3 AF488 (clone: 17A2, Biolegend, #100210, Mouse), mCD4 BUV395 (clone: GK1.5, BD, #563790, Mouse), mCD4 FITC (clone: GK1.5, BD, #553729, Mouse), mCD8 PE-Cy7 (Clone: 53-6.7, Biolegend, #100722, Mouse), hCD87 APC (clone VIM5, eBioscience, #17-3879-42. Human), muPAR PE (R&D Systems, FAB531P. Mouse), muPAR AF700 (R&D Systems, FAB531N. Mouse), huPAR (R&D. AF807. Human), muPAR (R&D. AF534. Mouse), mNRAS (Santa Cruz. SC-31. Mouse, rat, human), mSMA (abcam. Ab5694. Mouse, rat,chicken, piig, cow,dog, human, guinea pig), mKATE (Evrogen. ab233. All species), hCD3 (abcam. ab5690. Human), myc-tag (Cell Signaling. 2276S. All species), mKi-67 (abcam, ab16667.Mouse, rat, human, common marmoset), mIL-6 (abcam. ab6672. Human, monkey), p16-INK4A (Proteintech. 10883-1-AP. Human, monkey), mP-ERKT202/Y204 (Cell Signaling.4370. Human, mouse, rat, hamster, monkey, miink, D.melanogaster, zebrafish, pig, S.cerevisiae), desmin (ThermoFisher Scientific . RB-9014. Mouse, Human). All used antibodies are commercially available.

Eukaryotic cell lines

Policy information about cell lines

Cell line source(s)

ATCC (NALM6, human primary melanocytes). KP cells were a gift from Tyler Jacks. Eu-ALL01 were a gift from Renier J.Brentjens.

Authentication

COA with short tandem repeat was provided with cell line by ATCC. No other authentication was performed. Morphology and properties of all the cell lines pertinent to the experiments (e.g antigen expression or GFP-Luciferase expression) were routinely confirmed by flow cytometry.

Mycoplasma contamination

All cell lines were tested for mycoplasma and were found to be negative.

Commonly misidentified lines
(See ICLAC register)

No commonly misidentified cell lines were used.

Animals and other organisms

Policy information about studies involving animals; ARRIVE guidelines recommended for reporting animal research

Laboratory animals

NSG (NOD.Cg-Prkdc<scid>Il2rg<tm1Wjl>SzJ) mice male, 8-12 weeks old and obtained from the Jackson Laboratory. C57BL/6N mice were males and females, 8-12 weeks old and obtained from the Jackson Laboratory. B6.SJL-Ptrca/BoyAiTac were females, 6-8 weeks old and obtained from Taconic.

Wild animals

This study did not involve wild animals.

Field-collected samples

This study did not involve samples collected from the field.

Ethics oversight	Memorial Sloan Kettering Cancer Center (MSKCC) Internal Animal Care and Use Committee.

Note that full information on the approval of the study protocol must also be provided in the manuscript.

Human research participants

Policy information about studies involving human research participants

Population characteristics	Buffy coats from anonymous healthy donors were purchased from the New York Blood Center. The researchers were blind to any covariate characteristics. Samples from liver fibrosis were obtained from patients with a diagnosis of hepatitis C or B, alcoholic hepatitis or non-alcoholic steatohepatitis from the Biorepository and Pathology CoRE, (Icahn School of Medicine at Mount Sinai). Samples from normal pancreas and pancreatic tissue with PanIN were obtained from cases with a confirmed diagnosis of pancreatic ductal adenocarcinoma from the Department of Pathology at Memorial Sloan Kettering Cancer Center. Samples from human carotid sections were obtained from patients undergoing endarterectomy through the Department of Pathology at Weill Medical College of Cornell University.
Recruitment	Buffy coats were purchased from the New York Blood Center. Samples from liver fibrosis were obtained from patients with a confirmed diagnosis of hepatitis C or B, alcoholic hepatitis or non-alcoholic steatohepatitis. Samples were selected by pathologists at the Biorepository and Pathology CoRE, Icahn School of Medicine at Mount Sinai from their archive. Samples from normal pancreas and pancreatic tissue with PanINs were selected from cases with a confirmed diagnosis of pancreatic ductal adenocarcinoma. Samples were selected by pathologists at the Department of Pathology at Memorial Sloan Kettering Cancer Center from their archive. Samples from human carotid sections were obtained from patients undergoing endarterectomy as described in Peerschke, E.I.B. et al. Molecular Immunology. 41; 759-766 (2004): these were all patients with atherosclerotic lesions of type V according to the classification of the American Heart Association. No systematic bias likely to impact results were known at the time of data analysis for any of the samples.
Ethics oversight	All human studies were approved by Mount Sinai, or Weill Medical College of Cornell, or Memorial Sloan-Kettering Institutional Review Board.

Note that full information on the approval of the study protocol must also be provided in the manuscript.

Flow Cytometry

Plots

Confirm that:

☒ The axis labels state the marker and fluorochrome used (e.g. CD4-FITC).

☒ The axis scales are clearly visible. Include numbers along axes only for bottom left plot of group (a 'group' is an analysis of identical markers).

☒ All plots are contour plots with outliers or pseudocolor plots.

☒ A numerical value for number of cells or percentage (with statistics) is provided.

Methodology

Sample preparation	Buffy coats from anonymous healthy donors and peripheral blood from healthy volunteers were isolated and purified as described in Methods. For analysis of T cells in the livers, livers were dissociated using MACS Miltenyi Biotec liver dissociation kit (130-1-5-807), filtered through a 100µm strainer, washed with PBS, and red blood cell lysis was achieved with an ACK (Ammonium-Chloride-Potassium) lysing buffer (Lonza). Cells were washed with PBS, resuspended in PEB buffer and used for subsequent analysis. Lungs were minced and digested with 1mg/ml collagenase type IV and DNase type IV in RPMI at 37C and 200rpm for 45 minutes, filtered through 100µm strainer, washed with PBS, and red blood cell lysis was achieved with an ACK lysing buffer (Lonza). Cells were washed with PBS, resuspended in FACS buffer and used for subsequent analysis. For bone marrow samples, tibia and femurs were mechanically disrupted with a mortar in PBS/2mM EDTA, filtered through 40µm strainer, washed with PBS/2mM EDTA and red blood cell lysis was achieved with an ACK lysing buffer (Lonza). Cells were washed with PBS/2mM EDTA, resuspended in FACS buffer and used for subsequent analysis. Spleens were mechanically disrupted with the back of a 5-ml syringe, filtered through 40µm strainer, washed with PBS/2mM EDTA and red blood cell lysis was achieved with an ACK lysing buffer (Lonza). Cells were washed with PBS/2mM EDTA ,resuspended in FACS buffer and used for subsequent analysis. Cells were subsequently washed, resuspended in FACS Buffer with FcR blocking reagent; antibodies were added and washed off after the incubation time. If intracellular staining was performed, cells were fixed and permeabilized using the Cytofix/Cytoperm kit (BD Biosciences) or Intracellular Fixation & Permeabilizatiion Buffer Set Kit (eBioscience, #88-8824-00) according to the manufacturer's instructions. If cells were counted, counting beads (Invitrogen) were added in the final cell suspension to quantify cells. For analysis of live cells, 7-AAD (BD, #559925, Lot: 9031655, 1:40), Fixable Viability Dye eFluor 506 (65-0866-18, eBioscience, Lot: 2095423, 1:200) and LIVE/DEAD Fixable Violet (L34963, Invitrogen, Lot: 1985351, 1:100) were used.
Instrument	LSRII, BD. Fortessa 3,BD. Cytek Aurora (CYTEK)
Software	Collection: FACS DIVA.

Software	Analysis: Flowjo 10.1
Cell population abundance	The purity was verified by flow cytometry.
Gating strategy	The starting cell population was gated on a SSC-A/FSC-A plot. Cell singlets were identified by FSC/SSC gating. Positive/Negative populations were determined by FMO controls.

☒ Tick this box to confirm that a figure exemplifying the gating strategy is provided in the Supplementary Information.